RESEARCH ARTICLE | MARCH 08 2023
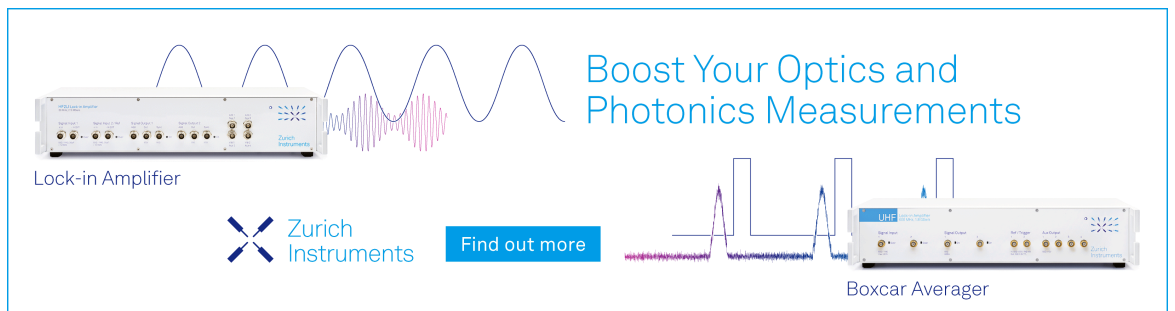
General weak segregation theory with an application to monodisperse semi-flexible diblock copolymers

P. M. Jager ⬤ ; W. J. Briels ⬤ ; J. J. M. Slot ✉ ⬤

Check for updates

View Online   Export Citation

General weak segregation theory with an application to monodisperse semi-flexible diblock copolymers

View Online   Export Citation   CrossMark

P. M. Jager,[1] [iD] W. J. Briels,[2,a) [iD] and J. J. M. Slot[3,b) [iD]

AFFILIATIONS

[1] EY, Centre for Tax and Legal Knowledge, Boompjes 258, P.O. Box 2295, 3011 XZ Rotterdam, The Netherlands

[2] MESA+ Institute for Nanotechnology, University of Twente, P.O. Box 217, 7500 AE Enschede, The Netherlands

[3] Department of Mathematics and Computer Science, CASA/Applied Analysis, Eindhoven University of Technology, P.O. Box 513, 5600 MB Eindhoven, The Netherlands

[a)] **Also at:** Forschungszentrum Jülich, IBI-4, D-52425 Jülich, Germany.
[b)] **Author to whom correspondence should be addressed:** j.j.m.slot@tue.nl

ABSTRACT

A general theory has been developed for a polydisperse semi-flexible multi-block copolymer melt. Using the Bawendi–Freed approach to model semi-flexible chains, an expression for the Landau free energy is derived in the weak segregation regime, which includes density and orientation order-parameters. The orientation order-parameter is described in the smectic phase and in more complicated structures, such as the hexagonal phase. The Landau free energy contains contributions of two kinds of interactions. The first kind is the Flory–Huggins interaction, which describes the incompatibility of chemically different blocks and may induce microphase separation. The second kind is the Maier–Saupe interaction, which may induce nematic ordering. In the framework of the weak segregation limit, the Landau theory allows us to predict phase structures in the melt as a function of the composition, persistence length, and the strength of the Flory–Huggins and Maier–Saupe interaction. The general theory is applied to a simple system of monodisperse semi-flexible diblock copolymers. In several phase diagrams, a number of possible phase structures are predicted, such as the bcc, hexagonal, smectic-A, smectic-C, and nematic phase. The influence of the Maier–Saupe interaction on the microphase structure is thoroughly discussed.

I. INTRODUCTION

In the last 50 odd years, the phase behavior of diblock copolymers and other sorts of block copolymers has been abundantly studied from both a theoretical (Refs. 1–40) and experimental perspective (Refs. 41–45). This phase behavior largely determines various properties of these materials, such as mechanical, optical, and electrical. For instance, the industrially important class of synthetic elastomers known as thermoplastic elastomers consists of block copolymers. These materials, due to their phase structure, are, in fact, processable rubbers. In these materials, typically one type of block is capable of crystallizing at a high enough temperature above room temperature, while the blocks that do not crystallize behave elastically at such a temperature. The block that does crystallize

forms cross-links between chains, resulting in the formation of a network. Upon the disappearance of the cross-links due to melting at elevated temperatures, chains can again move freely with respect to one another so that the system behaves as a high viscosity liquid.[46]

In this paper, we develop a general theory of a polydisperse semi-flexible multi-block copolymer melt, which is an extension of the theory in Ref. 1. The theory is made very general so that it can be applied not only to simple systems but also to more complex systems, which are more realistic. In this paper, it is applied to the simplest system of monodisperse diblocks, but the application can be extended to more complex systems, such as monodisperse triblocks and polydisperse diblocks. The general theory describes a melt, which is an arbitrary mixture of multi-block copolymers. The main parameters are the mixture composition determined by the

number of chains n_s for each chain species s, the chain composition of species s determined by Ising-like variables $\sigma_s^\alpha(l)$ such that $\sigma_s^\alpha(l) \equiv 1$ when segment l is in a block of kind α and $\sigma_s^\alpha(l) \equiv 0$ otherwise, the bending stiffness λ_α of a block of kind α, the strength of the Flory–Huggins $\chi_{\alpha\beta}$ and Maier–Saupe $\omega_{\alpha\beta}$ interaction between blocks of kinds α and β, the wavenumber q_* of a phase structure, the symmetry properties of a phase structure defined by the set of wave vectors $H = \{\pm \underline{q}_1, \pm \underline{q}_2, \ldots\}$ with a fixed wavenumber $q_1 = q_2 = \ldots = q_*$, and the strength of the density Ψ_α and orientation Υ_α order-parameter of block α. The general theory is applied to a simple system of monodisperse semi-flexible diblocks to calculate the complete phase diagram. From the results of these calculations, it follows how the stiffness may influence the formation of different phase structures in a melt of block copolymers.

This paper is structured as follows: In Sec. II, we review the literature and identify shortcomings/limitations of existing theories. In the second half of Sec. II, we describe in general terms what changes we are going to make to the models that were discussed. A summary is given at the end of Sec. II. In Sec. III, we describe our model and apply it in Sec. IV to a limited set of characteristic examples. We end with a few remarks and conclusions.

II. REVIEW OF EXISTING MODELS

The effect of stiffness on monodisperse semi-flexible diblocks has also been investigated in Refs. 6–9 and 19. In Refs. 6 and 9, a rod–coil system is investigated, and in Refs. 7, 8, and 19, the diblock is semi-flexible. In all these papers, it appeared that both the spinodals $\chi_s L$ and $\omega_s L$ are lowered when one or both blocks in the diblock copolymer are made stiffer. The semi-flexibility is described in different ways in the above-mentioned papers. In the general theory in Sec. III of this paper, the Bawendi–Freed model is applied to describe semi-flexibility; see also Refs. 51–53. In Ref. 7, the Kratky–Porod model is applied (see Ref. 54), and Ref. 19 applies the Saitô model introduced in Ref. 55. In Singh's semi-flexible chain model,[8] a certain number of rods with a fixed length are connected to each other in which each rod can be set in any direction with respect to a neighboring rod. The bending stiffness is modeled by the rod length. The rod-part or semi-flexible blocks in the diblock chain in Refs. 6–9 and 19 may have a certain orientation in a microphase or nematic phase. In Refs. 7 and 19, the orientation is ignored, but in Refs. 6 and 8 and this paper, the orientation tensor has the form

$$Q_{ij}^\alpha(\underline{q}) = \left(n_i^\alpha n_j^\alpha - \frac{1}{3}\delta_{ij}\right)Q^\alpha(\underline{q}) \qquad \text{with} \qquad \alpha = A, B, \quad (1)$$

in which the assumption, $\underline{n}^A = \underline{n}^B = \underline{n}$, is made that the director vectors $\underline{n}^A$ and $\underline{n}^B$ of the A- and B-block cannot become different. In Holyst's rod–coil model,[9] this orientation tensor has not been used for rod-blocks. The six tensor components Q_{xx}, Q_{yy}, Q_{zz}, Q_{xy}, Q_{xz}, and Q_{yz} are considered as independent variables in the expression of the Landau free energy. In Refs. 6 and 9, the orientation of the coil-part in the rod–coil diblock copolymer is neglected.

In Refs. 7–13, the weak segregation theory is restricted to the calculation of the spinodal line, but in Refs. 5 and 6, and this paper, the complete phase diagram is calculated. Reenders and ten Brinke[6] calculated the phase diagrams of monodisperse rod–coil diblocks, which displayed various phases, which are also observed in Sec. IV in this paper. As mentioned earlier, the description according to

Eq. (1) is applied to the alignment of rod-blocks in Ref. 6. Here, the ansatz is made that only global nematic ordering occurs so that contributions of orientation tensors $Q_{ij}^\alpha(\underline{q})$ to the Landau free energy are ignored for nonzero wave vectors $\underline{q} \neq \underline{0}$. In microphase structures in which $\chi > \chi_s$ and $\omega = 0$, only a global orientation may occur, but appear to be very small such that it is justified to also ignore these contributions. Therefore, in the calculation of the phase diagram, the tensor $Q_{ij}(\underline{q}) = Q_{ij}(\underline{0})$ is not included when $\omega < \omega_s$. Hence, a smectic phase only contains a global orientation and is only possible when both $\chi > \chi_s$ and $\omega > \omega_s$. However, in the theory, according to Refs. 8 and 9 and this paper, local orientations $Q_{ij}^\alpha(\underline{q})$ in which $\underline{q} \neq \underline{0}$ are not neglected in a microphase structure. Because of symmetry, the set of wave vectors applied to the density order-parameter $\Psi(\underline{q})$ must be identical to the set applied to the orientation order-parameter $Q_{ij}^\alpha(\underline{q})$ when a spatial dependent phase structure is formed. Hence, according to this theory, local orientations $Q_{ij}^\alpha(\underline{q})$ in several directions are possible when $\chi > \chi_s$ and $\omega = 0$. Global orientations $Q_{ij}^\alpha(\underline{0})$ may also be induced, which must be aligned along the wave vectors of the local orientations to maintain symmetry.

In Refs. 1–18, the phase behavior is described by the weak segregation theory, which is only valid just below to the critical temperature. When the temperature is further lowered, the segregation becomes stronger such that the weak segregation approach fails to be reliable. The phase structure is in the intermediate or strong segregation domain for which other approaches are available, for example, the self-consistent field theory in Refs. 19–36 or computer simulations in Refs. 37–40. In weak segregation, some results of the phase behavior found in Refs. 1–18 are observed in experiments; see also Refs. 41–45. In this paper, we restrict to the weak segregation approximation. In the past, this approximation has been applied in several kinds of block copolymers systems in which persistence length and/or polydispersity are included. In Refs. 14–18, the effect of polydispersity is investigated for different kinds of block copolymers, but the work of Refs. 5–13 and this paper are restricted to monodisperse systems in the framework of the weak segregation limit. The monodisperse systems in Refs. 5–10 and this paper are diblock copolymers. Monodisperse triblock copolymers are considered in Refs. 11 and 12. In Ref. 13 a melt of monodisperse side-chain liquid-crystalline polymers is investigated.

In this paper, we show and discuss the results of the calculated phase diagrams of monodisperse semi-flexible diblocks. Before discussing the results, we explain how we developed a general theory of a polydisperse semi-flexible multi-block copolymer melt, which is, as mentioned earlier, an extension of the theory in Ref. 1. In that paper, the polydisperse multi-block copolymers are fully flexible. In our paper, each chain is made semi-flexible by adding a persistence length or bending stiffness λ_a to each block α. If $\lambda_a \to 0$ block a, it can be regarded as fully flexible, and if $\lambda_a \to \infty$, it behaves as a rigid rod (see Refs. 56 and 57). Due to the persistence length of each block, it is necessary to take into account a possible global orientation of blocks induced by the Maier–Saupe interaction (see Ref. 50). The Flory–Huggins interaction might cause a space dependent alignment in a microphase state in addition to a space dependent density order-parameter. The theory in Ref. 1 is further extended by including this additional orientation expressed by the tensor Q_{ij}^α with $i, j = x, y, z$ and $\alpha = a, b, \ldots$ in the derivation of the Landau

free energy. The final result is a power series expansion in which two kinds of order-parameters are combined, which are density order-parameters Ψ^α and orientation tensors Q_{ij}^α.

To make chains semi-flexible, we use the continuous Bawendi–Freed model in Refs. 51–53 in which the chain can be stretched and compressed such that the chain length varies around a fixed average value L. In this way, the average distance l between a monomer and a chain end is also fixed if we measure the distance along the chain. Hence, by the length l, each monomer can be identified. If l is the real length instead of the average length, then the tangent vector $\underline{u}(l) = \frac{dr(l)}{dl}$ has a fixed magnitude equal to 1. This restriction obstructs the derivation of single-chain correlation functions. By using the average length, the tangent vector $\underline{u}(l)$ has no fixed unit magnitude. Only the average magnitude is fixed to 1. This condition is less strict such that the obstruction is taken away to derive explicit expressions of the single-chain correlation functions using the Bawendi–Freed model. This derivation and a detailed explanation of the Bawendi–Freed model can be found in Sec. I of the supplementary material. The resulting single-chain correlation functions are applied in the derivation of the Landau free energy; see also Sec. III and Appendix A. In Appendix B, the Landau free energy is derived for a simple system of diblock copolymers using the general theory in Sec. III and Appendix A. In this system, bending stiffness is included, but polydispersity is not taken into account. Here, the second order terms in the Landau free energy are written in matrix form and can be rewritten in terms of eigenvalues and eigenvectors. The three-dimensional symmetric matrix has three positive eigenvalues in the disordered state, but in the ordered state close to the phase transition, one eigenvalue has become negative. The corresponding eigenvector is called the primary eigenvector. The other eigenvectors are secondary eigenvectors. By minimizing the Landau free energy with respect to the secondary eigenvectors, the Landau free energy can be written as a power series expansion in only the primary eigenvector. This expression is used to minimize the free energy in different ordered structures, such as the bcc phase. The state with the lowest minimum is the most probable state. In this way, the phase diagram is calculated. As mentioned earlier in the expression of the free energy, a space dependent orientation tensor is included because it is necessary to take into account the possibility of local alignment in a certain microphase structure. In Appendix C, it is explained how the orientation tensor can be composed if the alignment is space dependent. Such an alignment, as explained earlier, is taken into account in microphase structures. It appeared that the orientation tensor of the hexagonal phase can be described as a superposition of three orientation tensors of smectic-A states. These three layered structures must be positioned such that the total combination contains the symmetrical properties conforming the hexagonal structure. In the same way, the bcc structure is a superposition of six orientation tensors of smectic-A states.

Finally, we would like to summarize the benefits of the approach taken in this paper. First, the model from our previous paper[1] is extended such that semi-flexibility of blocks is included via an adaptation of the Bawendi–Freed version of the freely rotating chain model. This model makes the further derivation of the Landau free energy possible. In previous papers, approximations are introduced that prevent such a derivation or model stiffness by introducing rod-like blocks. Second, the general theory is applied to

a simple system of monodisperse diblock copolymers in which the complete phase diagram has been calculated and investigated more extensively than in earlier papers in which the weak segregation theory is also applied. A spatial dependent orientation has been taken into account and is described in the smectic phase and more complicated structures, such as the hexagonal phase. This description is applied in the calculation of the complete phase diagram, which has not been done before. In this way, we are able to investigate the effect of stiffness on the complete phase diagram by means of a complete description of orientation.

III. THE MODEL

In this section, we develop a general theory of a polydisperse semi-flexible multi-block copolymer melt. Certain steps in the derivation of the resulting form of the Landau free energy given by Eq. (20) are not described thoroughly. For more details, we refer to Appendix A and the supplementary material, Secs. I–IV. The general theory in this paper is to a large extent based on earlier work, which can be found in Ref. 58.

We will describe a general melt of semi-flexible multi-block copolymers by employing the kind of *coarse graining* that one often finds in polymer physics.[59] Consider a melt in a volume V consisting of n_c copolymer chains that are built from up-to M chemically different kinds of monomers arranged in an arbitrary sequential way. Hence, these chains typically will have a multi-block-type structure, and the number of conceivable chains will be extremely large clearly. The subscript s will be used to label the different species of chains that are present in the system. Every chain of species s contains $N_s + 1$ monomers that are connected via N_s deformable bonds having an average length a and with a bond angle between subsequent bonds that is held fixed. In addition, we will allow this fixed angle between subsequent bonds to be different for each of the M chemically different blocks of monomers. Monomers will often also be called segments, and both names will be used interchangeably. These M chemically different segments will be labeled by Greek lowercase symbols α, β, etc. that run from 1 to M. In the remainder of this paper, a continuous notation will be used, i.e., we will represent chains by continuous curves that are obtained via the continuum limit ($N_s \to \infty$, $a \to 0$ such that $L_s \equiv N_s a$ stays constant, etc.). The structure of a given chain of species s is described by variables $\sigma_s^\alpha(l)$, where $\alpha = 1, \ldots, M$ and $l \in [0, L_s]$. These variables are similar to Ising spins in that $\sigma_s^\alpha(l) \equiv 1$ if segment l is of the α type and $\sigma_s^\alpha(l) \equiv 0$ if it is not. The continuous parameter l can be regarded not only as a parameter to label segments but also as a measure of the separation distance between one of the chain ends and the given segment measured along the chain. According to the supplementary material, Sec. I, l is not the actual contour length, but the average distance, as in the Bawendi–Freed model segments, has a variable length due to springs that couple these segments. The conformations of all the chains of species s are specified by listing both the set of spatial positions of the corresponding segments of each of the chains and the set of tangent vectors along the contours of the chains, i.e., the set $\{\underline{R}_m^s(l) \mid 0 \leqslant l \leqslant L_s, m = 1, \ldots, n_s\}_s$ defined with respect to some origin O in V and the set $\{\underline{u}_m^s(l) \equiv \underline{\dot{R}}_m^s(l) \equiv \frac{\partial R_m^s(l)}{\partial l} \mid 0 \leqslant l \leqslant L_s, m = 1, \ldots, n_s\}_s$. As bonds do not have a fixed length, tangent vectors are not unit vectors at every position along the contours of the chains. However, these

tangent vectors happen to be unit vectors in an averaged sense, as is shown in the supplementary material, Sec. I. A configuration or *micro-state* of the total system, denoted by γ, is defined by the full set $\{\underline{R}_m^s(l), \underline{u}_m^s(l) \mid 0 \leqslant l \leqslant L_s\}_{sm}$. Every *state-variable* G, i.e., every function of these micro-states, we will denote by $\hat{G} \equiv G(\gamma)$. Two examples of a state-variable that are relevant in the sequel are the so-called *microscopic α-segment density* $\hat{\rho}^\alpha(\underline{x})$, defined at each point $\underline{x} \in V$ by

$$\hat{\rho}^\alpha(\underline{x}) \equiv \sum_{sm} \int_0^{L_s} dl \; \sigma_s^\alpha(l) \; \delta(\underline{x} - \underline{R}_m^s(l)), \qquad (2)$$

and the *total microscopic segment density* $\hat{\rho}(\underline{x})$ is defined by

$$\hat{\rho}(\underline{x}) \equiv \sum_\alpha \hat{\rho}^\alpha(\underline{x}) = \sum_{sm} \int_0^{L_s} dl \; \delta(\underline{x} - \underline{R}_m^s(l)). \qquad (3)$$

By integrating these densities over V, we obtain, respectively, the total number of α-segments N^α and the overall number of segments N in the system. This last number can be either written as $\sum_\alpha N^\alpha$ or as $\sum_s n_s N_s$. Thus, the fraction of α-segments is given by $f^\alpha \equiv \frac{N^\alpha}{N}$. Without loss of generality, we will choose our length-scale in such a way that each segment has a unit volume and, therefore, that $N \equiv V$. In that case, it follows that

$$\frac{1}{V} \int_V d^3x \; \hat{\rho}(\underline{x}) \equiv 1 \qquad (4)$$

and that f^α can be written as

$$f^\alpha \equiv \frac{1}{V} \int_V d^3x \; \hat{\rho}^\alpha(\underline{x}). \qquad (5)$$

In order to describe the semi-flexibility of the copolymer chains, it is necessary to introduce, in addition, the so-called *microscopic α-segment orientation-tensor density* $\underline{\underline{\hat{S}}}^\alpha(\underline{x})$, which is given by

$$\underline{\underline{\hat{S}}}^\alpha(\underline{x}) \equiv \sum_{sm} \int_0^{L_s} dl \; \sigma_s^\alpha(l) \; \underline{u}_m^s(l) \; \underline{u}_m^s(l) \; \delta(\underline{x} - \underline{R}_m^s(l)), \qquad (6)$$

in case the tangent vectors are strictly unit vectors. As mentioned earlier, the magnitude of these vectors are only 1 on average. Hence, the definition according to Eq. (6) actually leads to an approximate segment orientation tensor. The repulsive nature of the interaction potentials at short distances between segments either in the same chain or in different chains, also referred to as *excluded volume*, is modeled approximately by assuming the system to be *incompressible*, i.e., to assume the total microscopic segment density $\hat{\rho}(\underline{x})$ to be equal to 1 at every $\underline{x} \in V$. The derivation of a Landau free energy for the general copolymer melt that is considered here, i.e., comprising of copolymer chains built from M *quasi-components*,[63] requires the introduction of, in total, $2M$ *order-parameters* or more precise $2M$ *order-parameter fields* to describe the various *inhomogeneous and anisotropic phases* the system can be found in and calculate the free energy of these states. These $2M$ order-parameter fields are course-grained versions of two sets of *microscopic order-parameter fields*, namely, a set of scalar fields,

$$\hat{\psi}^\alpha(\underline{x}) \equiv \hat{\rho}^\alpha(\underline{x}) - f^\alpha \qquad (\alpha = 1, \ldots, M), \qquad (7)$$

and a set of tensor fields,

$$\underline{\underline{\hat{Q}}}^\alpha(\underline{x}) \equiv \underline{\underline{\hat{S}}}^\alpha(\underline{x}) - \frac{1}{3}\hat{\rho}^\alpha(\underline{x})\underline{\underline{I}} \qquad (\alpha = 1, \ldots, M). \qquad (8)$$

Clearly, incompressibility, i.e., $\hat{\rho}(\underline{x}) = \sum_\alpha \hat{\rho}^\alpha(\underline{x}) = 1$, forces only $M - 1$ of the scalar fields to be independent because this condition implies that

$$\sum_\alpha \hat{\psi}^\alpha(\underline{x}) \equiv 0. \qquad (9)$$

Interactions between the segments within the same chain or between segments in different chains in this copolymer melt can be formulated using these microscopic order-parameter fields. For this, assume that these interactions only occur between pairs of segments and, hence, are pairwise additive. In that case, one can write the total interaction energy $\hat{W}$ of the system as

$$\hat{W} \equiv \frac{1}{2} \sum_{\alpha\beta} \sum_{sm} \sum_{s'm'} \int_0^{L_s} dl \int_0^{L_{s'}} dl' \; \sigma_s^\alpha(l) \; \sigma_{s'}^\beta(l')$$
$$\times w_{\alpha\beta}(\underline{R}_m^s(l) - \underline{R}_{m'}^{s'}(l') \, ; \underline{u}_m^s(l) \cdot \underline{u}_{m'}^{s'}(l')), \qquad (10)$$

in which $w_{\alpha\beta}(\underline{x} \, ; \underline{u} \cdot \underline{u}')$ is the interaction potential between a segment of type α and a segment of type β. This potential is assumed to be short-ranged in space, i.e., $w_{\alpha\beta}(\underline{x} \, ; \underline{u} \cdot \underline{u}') \simeq \widetilde{w}_{\alpha\beta}(\underline{u} \cdot \underline{u}') \, \delta(\underline{x})$. In addition, $\widetilde{w}_{\alpha\beta}(\underline{u} \cdot \underline{u}')$ can be expanded in the following way:

$$\widetilde{w}_{\alpha\beta}(\underline{u} \cdot \underline{u}') = \varepsilon_{\alpha\beta} - \omega_{\alpha\beta} \; (\underline{u} \cdot \underline{u}')^2 + \cdots. \qquad (11)$$

In this expansion, terms of the form $(\underline{u} \cdot \underline{u}')^k$ with k odd are absent due to the assumed symmetry of the segments (fore-aft symmetry). In the expression for $\hat{W}$ (10), also terms with $\alpha = \beta$, $s = s'$, $m = m'$, and $l = l'$ are formally included. These so-called "self-energy" terms should not be present, but we will not alter the notation to explicitly remove them from the expression. After the substitution of (11) into (10), the resulting expression for $\hat{W}$ can be rewritten using the microscopic segment densities $\hat{\rho}^\alpha(\underline{x})$ (2) and $\underline{\underline{\hat{S}}}^\alpha(\underline{x})$ (6) in the form of

$$\hat{W} \simeq \frac{1}{2} \sum_{\alpha\beta} \varepsilon_{\alpha\beta} \int_V d^3x \; \hat{\rho}^\alpha(\underline{x}) \, \hat{\rho}^\beta(\underline{x})$$
$$- \frac{1}{2} \sum_{\alpha\beta} \omega_{\alpha\beta} \int_V d^3x \; \underline{\underline{\hat{S}}}^\alpha(\underline{x}) : \underline{\underline{\hat{S}}}^\beta(\underline{x}). \qquad (12)$$

Upon the elimination of one of $\hat{\rho}$'s, say, $\hat{\rho}^M$, from (12) using $\sum_\alpha \hat{\rho}^\alpha(\underline{x}) \equiv 1$, and substitution of $\hat{\rho}^\alpha(\underline{x}) = \hat{\psi}^\alpha(\underline{x}) + f^\alpha$ and $\underline{\underline{\hat{S}}}^\alpha(\underline{x}) = \underline{\underline{\hat{Q}}}^\alpha(\underline{x}) + \frac{1}{3}\hat{\rho}^\alpha(\underline{x})\underline{\underline{I}}$, one ends up with

$$\hat{W} \simeq \frac{1}{2} \sideset{}{'}\sum_{\alpha\beta} E_{\alpha\beta} \int_V d^3x \; \hat{\psi}^\alpha(\underline{x})\hat{\psi}^\beta(\underline{x})$$
$$- \frac{1}{2} \sum_{\alpha\beta} \omega_{\alpha\beta} \int_V d^3x \; \underline{\underline{\hat{Q}}}^\alpha(\underline{x}) : \underline{\underline{\hat{Q}}}^\beta(\underline{x})$$
$$- \frac{1}{3} \sum_{\alpha\beta} \omega_{\alpha\beta} \int_V d^3x \; (\hat{\psi}^\alpha(\underline{x}) + f^\alpha) \operatorname{Tr} \underline{\underline{\hat{Q}}}^\beta(\underline{x}) \qquad (13)$$

with $\quad E_{\alpha\beta} \equiv \varepsilon'_{\alpha\beta} - \varepsilon'_{\alpha M} - \varepsilon'_{\beta M} + \varepsilon'_{MM} \quad$ and $\quad \varepsilon'_{\alpha\beta} = \varepsilon_{\alpha\beta} - \frac{1}{3}\omega_{\alpha\beta}$. The prime in the first term of $\hat{W}$ implies that both sums run from 1 to $M-1$. In terms of the set of Flory χ-parameters[47] between the different segments, i.e.,

$$\chi_{\alpha\beta} \equiv \varepsilon_{\alpha\beta} - \frac{\varepsilon_{\alpha\alpha} + \varepsilon_{\beta\beta}}{2} \qquad \text{with} \qquad \chi_{\alpha\alpha} = 0, \forall \alpha, \qquad (14)$$

this $E_{\alpha\beta}$ can be written as

$$E_{\alpha\beta} = \chi_{\alpha\beta} - \chi_{\alpha M} - \chi_{\beta M} \equiv -2\,\tilde{\chi}_{\alpha\beta}, \qquad (15)$$

and, thus, we can write $\hat{W}$ as

$$\begin{aligned}
\hat{W} \simeq &-\sum_{\alpha\beta}{}' \tilde{\chi}_{\alpha\beta} \int_V d^3x \; \hat{\psi}^\alpha(\underline{x}) \hat{\psi}^\beta(\underline{x}) \\
&- \frac{1}{2}\sum_{\alpha\beta} \omega_{\alpha\beta} \int_V d^3x \; \underline{\hat{Q}}^\alpha(\underline{x}) : \underline{\hat{Q}}^\beta(\underline{x}) \\
&- \frac{1}{3}\sum_{\alpha\beta} \omega_{\alpha\beta} \int_V d^3x \; (\hat{\psi}^\alpha(\underline{x}) + f^\alpha) \operatorname{Tr} \underline{\hat{Q}}^\beta(\underline{x}).
\end{aligned} \qquad (16)$$

In the binary case ($M = 2$), there is only one $\tilde{\chi}$-parameter, $\tilde{\chi}_{11}$, which is equal to χ_{12}. The next step is the formulation of the *partition function Z* of the copolymer melt on the basis of the interaction energy (16). This requires, in addition, a specification of the *unnormalized statistical weight* $e^{-\hat{H}_0}$ (using units for which $k_B T = 1$) of the copolymer melt when the interactions are switched off. To describe chains that locally may have any degree of flexibility varying between that of a fully flexible chain all the way to that of a rigid-rod, we model the *unperturbed* semi-flexible copolymer melt by a statistical ensemble of Gaussian chains that are persistent locally, i.e., similar as in the Bawendi–Freed model.[52,53] The *unperturbed Hamiltonian* $\hat{H}_0$ is therefore defined by

$$\begin{aligned}
\hat{H}_0 \equiv &\frac{3}{4}\sum_{sm}\left\{\left[\underline{u}^s_m(0)\right]^2 + \left[\underline{u}^s_m(L_s)\right]^2\right\} + \frac{3}{4}\sum_{sm}\int_0^{L_s} dl \\
&\times \left\{\frac{1}{\lambda_s(l)}\left[\underline{u}^s_m(l)\right]^2 + \lambda_s(l)\left[\underline{\dot{u}}^s_m(l)\right]^2\right\},
\end{aligned} \qquad (17)$$

in which the local *persistence length* of the chains of type s is denoted by $\lambda_s(l)$. The form of this $\lambda_s(l)$ for a copolymer chain of the multiblock type is given by

$$\lambda_s(l) \equiv \sum_{i=1}^{N_s^b} \lambda_s^{(i)}\left[\theta\left(l - \sum_{j=1}^{i-1} L_s^{(j)}\right) - \theta\left(l - \sum_{j=1}^{i} L_s^{(j)}\right)\right], \qquad (18)$$

where $L_s^{(i)}$ and $\lambda_s^{(i)}$ denote the block length and persistence length, respectively, of the ith block in a chain of type s consisting of N_s^b blocks. The function $\theta(\cdots)$ in (18) between the square brackets is the Heaviside step function. The presence of the first term in (17), involving the orientation vectors of the endpoints of the chains, and the specific choice of the coefficients in the second term are to ensure both homogeneity of the chains and averaged kind of Porod–Kratky behavior, i.e., $\langle[\underline{u}^s_m(l)]^2\rangle_0 = 1, \quad \forall l \in [0, L_s]$. $\langle\cdots\rangle_0$ here denotes averaging over all allowable configurations of a single free chain. For its definition, see Eq. (A14) in Appendix A.

In the supplementary material, Sec. I, it is explained that in the Bawendi–Freed approach, the semi-flexible chain can be regarded as a chain of harmonic oscillators in which the segments are connected by springs. Due to the springs, the length of the tangent vector is only on average a unit vector, so as mentioned earlier, $\langle[\underline{u}^s_m(l)]^2\rangle_0 = 1, \forall l \in [0, L_s]$. This less strict condition makes it possible to derive the single-chain correlation functions. This derivation is described in detail in the supplementary material, Sec. I. The single-chain correlation functions are determined in Appendix A in which also the final expression for the Landau free energy Eq. (20) is derived.

The full Hamiltonian $\hat{H}$ for a particular configuration of the copolymer melt is the sum of the unperturbed Hamiltonian $\hat{H}_0$ and the total interaction energy $\hat{W}$,

$$\hat{H} = \hat{H}_0 + \hat{W}. \qquad (19)$$

Each configuration γ contributes the term $\exp(-\hat{H})$, the so-called *Boltzmann weight*, to the partition function Z. In Appendix A, Z, written as a functional integral over all possible configurations, is evaluated. The Landau free energy F_L is derived from this partition function by determining the most dominant contribution to Z. The configuration that gives this dominant contribution is the most probable configuration, i.e., the equilibrium state of the melt. The corresponding free energy (in units of $k_B T$) is the Landau free energy written in terms of the Fourier transform of the order-parameter fields,

$$\begin{aligned}
\frac{F_L}{V} = \min_{\Psi, \Upsilon} \Big\{ &(\Gamma^{(2)}_{ab} - \tilde{\chi}_{ab})\Psi^a\Psi^b + 2\Gamma^{(2)}_{a\bar{b}}\Psi^a\Upsilon^{\bar{b}} + \Big(\Gamma^{(2)}_{\bar{a}\bar{b}} - \frac{1}{2}\omega_{\bar{a}\bar{b}}\Big)\Upsilon^{\bar{a}}\Upsilon^{\bar{b}} \\
&- \frac{1}{3}\omega_{ab}\Upsilon^{a,ij}\delta_{ij}(\Psi^b + f^b) + \Gamma^{(3)}_{abc}\Psi^a\Psi^b\Psi^c + 3\Gamma^{(3)}_{ab\bar{c}}\Psi^a\Psi^b\Upsilon^{\bar{c}} \\
&+ 3\Gamma^{(3)}_{a\bar{b}\bar{c}}\Psi^a\Upsilon^{\bar{b}}\Upsilon^{\bar{c}} + \Gamma^{(3)}_{\bar{a}\bar{b}\bar{c}}\Upsilon^{\bar{a}}\Upsilon^{\bar{b}}\Upsilon^{\bar{c}} + \Gamma^{(4)}_{abcd}\Psi^a\Psi^b\Psi^c\Psi^d \\
&+ 4\Gamma^{(4)}_{abc\bar{d}}\Psi^a\Psi^b\Psi^c\Upsilon^{\bar{d}} + 6\Gamma^{(4)}_{ab\bar{c}\bar{d}}\Psi^a\Psi^b\Upsilon^{\bar{c}}\Upsilon^{\bar{d}} + 4\Gamma^{(4)}_{a\bar{b}\bar{c}\bar{d}}\Psi^a\Upsilon^{\bar{b}}\Upsilon^{\bar{c}}\Upsilon^{\bar{d}} \\
&+ \Gamma^{(4)}_{\bar{a}\bar{b}\bar{c}\bar{d}}\Upsilon^{\bar{a}}\Upsilon^{\bar{b}}\Upsilon^{\bar{c}}\Upsilon^{\bar{d}} \Big\}
\end{aligned} \qquad (20)$$

with $\tilde{\chi}_{ab} \equiv \tilde{\chi}_{\alpha\beta}\,\delta(\underline{q}_1 + \underline{q}_2)$, $\omega_{\bar{a}\bar{b}} \equiv \omega_{\alpha\beta}\,|2\delta_{ii'}\delta_{jj'} - \delta_{ij}\delta_{i'j'}|\,\delta(\underline{q}_1 + \underline{q}_2)$, $\Psi^a \equiv \frac{\psi^\alpha(-\underline{q}_1)}{V}$, $\Upsilon^{\bar{a}} \equiv \frac{Q^\alpha_{ij}(-\underline{q}_1)}{V}$, and $f^b = f^\beta\delta(\underline{q}_2)$. In the expression for this free energy, we use the *composite labels* $a \equiv (\underline{q}_1 \neq \underline{0}, \alpha)$, $b \equiv (\underline{q}_2 \neq \underline{0}, \beta)$, etc. and $\bar{a} \equiv (\underline{q}_1, ij, \alpha)$, $\bar{b} \equiv (\underline{q}_2, i'j', \beta)$, etc. in which the pairs ij and $i'j'$ are one of the six unique pairs xx, yy, zz, xy, xz, and yz. The coefficient functions (Γ's) are known as *vertices* and are defined in Eqs. (II.14)–(II.16) of the supplementary material, Sec. II. In each term in Eq. (20), we see that each composite label in a subscript matches with a composite label in a superscript in one of the order-parameters. In such a match, the Einstein summation convention is used. The summation over the wave vectors $\underline{q}$ is limited over a set $H = \{\pm\underline{q}_1, \pm\underline{q}_2, \ldots\}$ in which all wave vectors have the same fixed magnitude q_*. This set H defines the symmetry properties and wavelength of a phase structure.[60–62]

In Appendix B, Eq. (20) is applied to a melt of monodisperse semi-flexible diblock copolymers in which there is only one Flory–Huggins interaction parameter $\chi_{AB} = \chi$ between A- and B-blocks. A microphase structure is formed when χ is strong enough

and above the spinodal χ_s. According to Appendix B, the earlier mentioned magnitude q_* follows from minimizing the spinodal expression given by Eq. (B9) with respect to the magnitude q_* of the wave vectors in set H. When we know q_*, we can calculate the complete expression of the Landau free energy for a certain phase structure with a set of wave vectors H, for example, the lamellar state in which $H = \{\pm q\}$. This complete expression is minimized with respect to the order-parameters. In the same way, the minimum free energy is calculated for other phase structures H. The phase structure with the lowest minimum is the most probable state of the melt. In this way, the phase diagram is calculated. When the persistence length of λ_A and λ_B is getting close to zero, then the diblocks become totally flexible. In that case, the expression of the Landau free energy given by Eq. (20) can be reduced to the expression derived in Ref. 5.

IV. RESULTS AND DISCUSSION

In this section, we present results of calculations of several phase diagrams of a system of diblock copolymers. The persistence length is varied in both the A- and B-blocks. Polydispersity is not taken into account. The phase diagrams are calculated using the expression of the Landau free energy in terms of eigenvectors and eigenvalues in Appendix B and the spatial orientation tensor according to Appendix C. The following systems have been investigated: (a) rod–coil system ($\lambda_A/L_A = 10^2 \gg \lambda_B/L_B = 10^{-4}$); (b) semi–coil system ($\lambda_A/L_A = 10^{-1} \gg \lambda_B/L_B = 10^{-4}$); and (c) semi–semi system ($\lambda_A/L_A = 10^{-1} = \lambda_B/L_B$).

Before we present and discuss the results, some remarks have to be made. The Maier–Saupe interaction strength and persistence length cannot be considered as independent according to Refs. 48 and 49. In a melt of rods, there is always alignment caused by the excluded volume effect and a disordered phase cannot be formed. A nonzero Maier–Saupe interaction is always present if the chains are semi-flexible, and it becomes stronger when the chains become stiffer. A disordered phase is still possible according to Refs. 48 and 49 if the persistence length is small enough and satisfies the condition $\frac{\lambda}{d} < 50$ in which d is the diameter of the chain. In Sec. III, we read that each monomer or segment has a unit volume so that d is ~1 and $\frac{\lambda}{d} \approx \lambda < 50$. This condition can be met in, for example,

the (c) semi–semi system ($\lambda_A/L_A = 10^{-1} = \lambda_B/L_B$) because the calculated phase diagrams are applicable to any arbitrary chain length L. We assume that the disordered state may also be formed in systems (a) and (b).

In Fig. 1, three phase diagrams are calculated for system (a). The contributions of the orientation Υ_B and Maier–Saupe parameters ω_{BB} and ω_{AB} are ignored because the B-block can be regarded as fully flexible. The remaining Maier–Saupe parameters ω_{AA} are used in the ratio $r = \frac{\omega_{AA}}{\chi} = \frac{\omega}{\chi}$, which has a fixed value in each phase diagram. These fixed ratios are 0.0, 0.4, and 0.7 in Figs. 1(a)–1(c), respectively. The fraction of A-blocks f^A defined by Eq. (5) is denoted as f in Fig. 1 and the rest of this section because we restrict to diblock copolymers. In all three phase diagrams in Fig. 1, χL and f are varied within the same interval. Increasing the ratio r has a strong effect on the formation of phase structures. In Fig. 1(a), the bcc structure can be found close to the spinodal in a very small part. The size increases at a larger r. The same effect can be observed for the hexagonal and smectic-A structure. The smectic-C structure is moved to a larger χ when r is increased.

To understand the effect of r observed in Fig. 1, the components Ψ_1 and Υ_1^A of the primary eigenvector $\underline{x}_1 = (\Psi_1, \Upsilon_1^A, \Upsilon_1^B)$ are investigated in each microphase structure at a certain point in the phase diagram where microphase separation is predicted. If we compare the density components $\Psi_{1,smecC}$, $\Psi_{1,smecA}$, $\Psi_{1,hex}$, and $\Psi_{1,bcc}$, we always see the following ordering:

$$|\Psi_{1,smecC}| \geq |\Psi_{1,smecA}| \geq |\Psi_{1,hex}| \geq |\Psi_{1,bcc}|. \quad (21)$$

The order of the orientation components $|\Upsilon_1^A|$ is

$$|\Upsilon_{1,smecC}^A| \geq |\Upsilon_{1,smecA}^A| \geq |\Upsilon_{1,hex}^A| \geq |\Upsilon_{1,bcc}^A|. \quad (22)$$

When r increases, it appears that both $|\Psi_{1,bcc}|$ and $|\Upsilon_{1,bcc}^A|$ become smaller. These components are also lowered by an increasing r in the hexagonal, smectic-A, and smectic-C phase. It can be concluded that the Maier–Saupe interaction ω weakens the separation of A- and B-blocks. We also see this weakening in the phase diagrams in which structures with lower components $|\Psi_1|$ and $|\Upsilon_1^A|$ become more dominant. Because the interaction ω stimulates alignment, we would expect that component $|\Upsilon_1^A|$ is enhanced by this interaction.
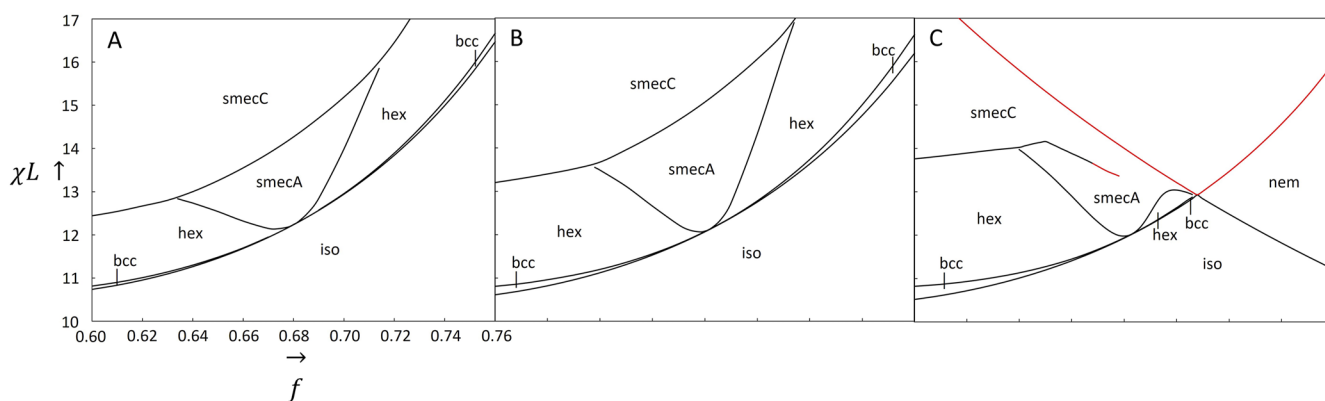
FIG. 1. Phase diagrams of a rod–coil diblock in which $\lambda_A/L = 10^2$; $\lambda_B/L = 10^{-4}$; and $r = 0.0$, 0.4, and 0.7. In (a), $r = 0.0$ is chosen; in (b), $r = 0.4$; and in (c), $r = 0.7$.

However, it is weakened. This component is a measure of space dependent alignment, but a strong enough ω causes nematic ordering, which is a global alignment. In a microphase structure, global alignment may still be possible without interaction ω, but is almost negligible because it is a contribution of a secondary eigenvector $\underline{x}_{10} = (\Upsilon_{10}^A, \Upsilon_{10}^B) \approx (\Upsilon_{10}^A, 0)$, which contains a global orientation Υ_{10}^A component. The secondary parameter $x_{10} = \pm |\underline{x}_{10}| \approx \pm |\Upsilon_{10}^A|$ is given by Eq. (B12) in which $n = 10$,

$$x_{10} = \frac{-C_{11,10}^{(3)} x_1^2}{2\lambda_{10}} + O(x_1^3). \tag{23}$$

If interaction ω is increased, the positive eigenvalue λ_{10} becomes smaller, which enhances the global orientation $|\Upsilon_{10}^A|$. This alignment becomes stronger when ω is getting close to the spinodal $\omega_s(q_* = 0)$ because then $\lambda_{10} \downarrow 0$. In the bcc structure, a global alignment is not possible, so $|\Upsilon_{10,bcc}^A| = 0$.

In the red line in Figs. 1(b) and 1(c), at least one of the interaction parameters χ or ω is equal to its spinodal value, so $\chi = \chi_s(q_* \neq 0)$ or $\omega = \omega_s(q_* = 0)$. In Fig. 1(c), at the point in the red line where $f = 0.71$, both $\chi = \chi_s(q_* \neq 0)$ and $\omega = \omega_s(q_* = 0)$. In that case, both eigenvalues λ_1 and λ_{10} in Eq. (B10) are zero so that both a microphase structure can be formed and global alignment is possible if the temperature is further lowered. In this situation, Eq. (B14) cannot be used anymore because it is valid only if the second order contribution in Eq. (B10) contains one negative eigenvalue λ_1 such that the Landau free energy can be written in terms of only one primary parameter x_1. If the second order contribution has two negative eigenvalues λ_1 and λ_{10}, then besides x_1, there is a second primary parameter x_{10} so that the free energy is expressed as

$$\begin{aligned}\frac{F_L}{V} = \min_{\{x_1, x_{10}\}} \Big\{ &\lambda_1 x_1^2 + \lambda_{10} x_{10}^2 + C_{111}^{(3)} x_1^3 + C_{11,10}^{(3)} x_1^2 x_{10} \\ &+ C_{10,10,10}^{(3)} x_{10}^3 + \widetilde{C}_{1111}^{(4)} x_1^4 + \widetilde{C}_{111,10}^{(4)} x_1^3 x_{10} + \widetilde{C}_{11,10,10}^{(4)} x_1^2 x_{10}^2 \\ &+ \widetilde{C}_{10,10,10,10}^{(4)} x_{10}^4 \Big\}, \end{aligned} \tag{24}$$

in which the fourth order coefficients depend on secondary eigenvalues λ_2, λ_3, and λ_{20},

$$\widetilde{C}_{1111}^{(4)} = C_{1111}^{(4)} - \sum_{n \neq 1,10} \frac{(C_{11n}^{(3)})^2}{4\lambda_n}, \tag{25a}$$

$$\widetilde{C}_{111,10}^{(4)} = C_{111,10}^{(4)} - \frac{C_{11,2}^{(3)} C_{1,10,2}^{(3)}}{2\lambda_2} - \frac{C_{11,3}^{(3)} C_{1,10,3}^{(3)}}{2\lambda_3}, \tag{25b}$$

$$\widetilde{C}_{11,10,10}^{(4)} = C_{11,10,10}^{(4)} - \frac{(C_{1,10,2}^{(3)})^2}{4\lambda_2} - \frac{(C_{1,10,3}^{(3)})^2}{4\lambda_3} - \frac{C_{11,20}^{(3)} C_{10,10,20}^{(3)}}{2\lambda_{20}}, \tag{25c}$$

and

$$\widetilde{C}_{10,10,10,10}^{(4)} = C_{10,10,10,10}^{(4)} - \frac{(C_{10,10,20}^{(3)})^2}{4\lambda_{20}}. \tag{25d}$$

By means of numerical calculations, it has been verified that $C_{1111}^{(4)}$ in Eqs. (B14) and (25a) is still positive if χ is just above χ_s, but becomes

negative if χ becomes too large so that we need higher order terms to find the minimum. This makes the primary parameter x_1 even larger and the mean field approximation even less reliable. The same problem occurs because of $C_{10,10,10,10}^{(4)}$ in Eq. (25d), which appears to be negative so that $\widetilde{C}_{10,10,10,10}^{(4)} x_{10}^4$ is also negative in Eq. (24). Hence, to minimize the free energy, Eq. (24) can only be applied below the red line in Figs. 1(b) and 1(c). Here, a smectic-C state is predicted. It is not plausible that a different structure is formed above the red line. A layered microphase state is expected in which the orientation $\underline{\underline{Q}}_\alpha (\underline{x})$ has not only a space dependent contribution but also a stronger global alignment $\underline{\underline{Q}}_\alpha^0$ because eigenvalue λ_{10} has also become negative. As a result, the components of the space average $\langle \underline{\underline{Q}}_\alpha (\underline{x}) \rangle$,

$$\langle \underline{\underline{Q}}_\alpha (\underline{x}) \rangle = \frac{1}{V} \int_V d^3 x \, \underline{\underline{Q}}_\alpha (\underline{x}) = \underline{\underline{Q}}_\alpha^0, \tag{26}$$

are not zero, in general. A global alignment x_{10} in combination with spatial alignment may also occur if ω is below the spinodal $\omega_s(q_* = 0)$. This global contribution x_{10} is given by Eq. (23) and belongs to the secondary eigenvector $\lambda_{10} > 0$, which is negligible if $\lambda_{10} \gg 0$. However, when λ_{10} reaches zero closer and closer, it cannot be neglected. At the same time, the fourth order term in Eq. (B14) is getting close to zero or may even become negative such that the weak segregation approximation according to Eq. (B14) cannot be applied anymore.

In Fig. 1(c) at $f = 0.65$, we see a discontinuity in the line that marks the transition from the smectic-A to the smectic-C phase or vice versa. Here, the angle θ is $13°$ if f is just below 0.65. Just above 0.65, it has jumped to $89.9°$. At the discontinuity, we are near the red line at which $\chi = \chi_s$ and/or $\omega = \omega_s$. As explained earlier, when we are getting closer to this red line, the positive eigenvalue λ_{10} is getting closer to zero so that the global alignment according to Eq. (23) is increasing. This alignment lowers the coefficient $\widetilde{C}_{1111}^{(4)}$ in Eq. (B14) such that the minimum is reached at $\theta = 89.9°$ instead of $\theta = 13°$. Between the discontinuity at $f = 0.65$ and 0.67, the transition line is black, but at $f > 067$, it is extrapolated by a red line to indicate that the mean field approximation according to Eq. (B14) is again not valid because λ_{10} reaches zero such that $\widetilde{C}_{1111}^{(4)} < 0$. However, if f is just below 0.67, the coefficient $\widetilde{C}_{1111}^{(4)}$ is positive, but very small such that a large primary parameter x_1 is found at the minimum in Eq. (B14). The larger the x_1, the less reliable the mean field approximation is.

In Ref. 8 the dependence of the spinodal χ_s and the corresponding wave mode q_* on the Maier–Saupe interaction has been investigated for semi-flexible monodisperse diblocks. It appeared that χ_s is lowered and q_* is increased by the Maier–Saupe interaction. The same effect is observed by calculating $\chi_s L$ and $q_* L$ as a function of $r = \frac{\omega}{\chi}$ using Eq. (B9) in this paper for monodisperse rod–coil diblocks. The relation between $\chi_s L$ and r and also between $q_* L$ and r appeared to be approximately linear. These two dependencies are hardly observed if the persistence length of the A- and B-block is identical, but these become stronger when the A-block gets stiffer and the B-block gets more flexible. Larger A- and B-rich domains are formed at a lower r because q_* is lowered. This reduces the boundary
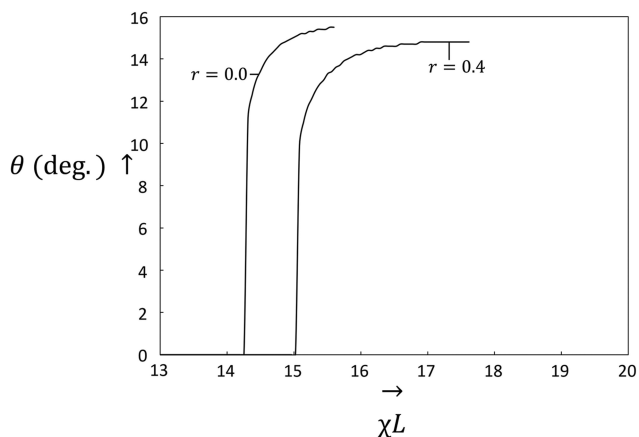
FIG. 2. The orientation angle θ in the smectic-C phase as a function of χL of a rod–coil diblock at $f = 0.68$.

area between A- and B-rich domains with respect to the melt volume such that a stronger separation is possible, which is a plausible explanation why $|\Psi_1|$ and $|\Upsilon_1^A|$ increase when lowering r. A stronger separation increases the enthalpic term $\widetilde{\chi}_{ab}\Psi^a\Psi^b$ in Eq. (20). However, the mixing entropy decreases. When $r = 0$, the domain size $\approx \frac{1}{q_*}$ reaches a maximum value to form a stable microphase structure. This structure would be instable if we reduce this size because the increased mixing entropy is not enough to compensate the loss of the enthalpic part $\widetilde{\chi}_{ab}\Psi^a\Psi^b$. However, when $r > 0$, the enthalpic part gets an additional alignment contribution $\frac{1}{2}\omega_{\overline{a}\overline{b}}\Upsilon^{\overline{a}}\Upsilon^{\overline{b}}$, which reduces the loss of enthalpy such that it is now in equilibrium with the increased mixing entropy. Hence, a stable microphase structure with smaller domains can be formed by means of the additional alignment contribution. This explains why q_*L decreases at a smaller r. At the same time, $\chi_s L$ increases for which the same explanation is applicable.

From the analysis and discussion of the phase behavior in Fig. 1, we earlier conclude that Maier–Saupe interaction reduces separation

of A- and B-blocks. The same conclusion follows from the spinodal calculations using Eq. (B9) because q_*L is increasing when r increases. However, the opposite effect also takes place because the spinodal χ_s is lowered when the parameter r is increasing. Hence, in that case, microphase separation is stimulated by the Maier–Saupe interaction. The stimulation takes place when the melt is close to the phase transition, but it is still in the disordered phase. When the spinodal χ_s is lowered, the disordered phase is converted into a microphase structure. However, the counteracting effect occurs when a microphase structure is already present before increasing the parameter r.

In Fig. 1, a smectic-A phase is found just above the critical point at $f = 0.68$ in which the orientation $\theta = 0°$. At a certain $\chi > \chi_s$, this phase is converted into a smectic-C state with a nonzero orientation θ. To investigate this orientation, we plot θ against χL in a graph at the critical point $f = 0.68$ for both $r = 0.0$ and 0.4 in Fig. 2. At $r = 0.7$, we do not investigate θ because in Fig. 1(c) at $f > 0.67$, the transition line between the smectic-A and smectic-C phase has been extrapolated by a red line to indicate that the mean field approximation according to Eq. (B14) in which $\widetilde{C}_{1111}^{(4)} < 0$ cannot be applied as explained earlier. In both graphs at a certain χL, the orientation θ makes a sudden jump in which intermediate values of θ are not possible. After the jump, θ increases continuously and is converging to a maximum θ at which the line is ended. After the end point, the coefficient $\widetilde{C}_{1111}^{(4)} < 0$ is below zero so that Eq. (B14) is not valid any more. We earlier conclude that the Maier–Saupe interaction reduces the separation of A- and B-blocks. This reduction also follows from Fig. 2 because when r is increased, the jump is shifted to a larger χL. Additionally, a smectic-C phase is formed with a smaller θ.

In Fig. 3, three phase diagrams are calculated for system (b) as mentioned in the beginning of this section. In the calculations of previous system (a), we explained that Υ_B, ω_{BB}, and ω_{AB} can be ignored. For the same reason, these parameters are excluded in system (b). In Figs. 3(a)–3(c), the ratio $r = \frac{\omega_{AA}}{\chi} = \frac{\omega}{\chi}$ is taken equal to 0, 3, and 5, respectively. In all three phase diagrams, χL and f are varied within the same interval. In Fig. 3(c), the points at which $\omega = \omega_s(q_* = 0)$ or $\chi = \chi_s(q_* \neq 0)$ are also indicated by a red line.
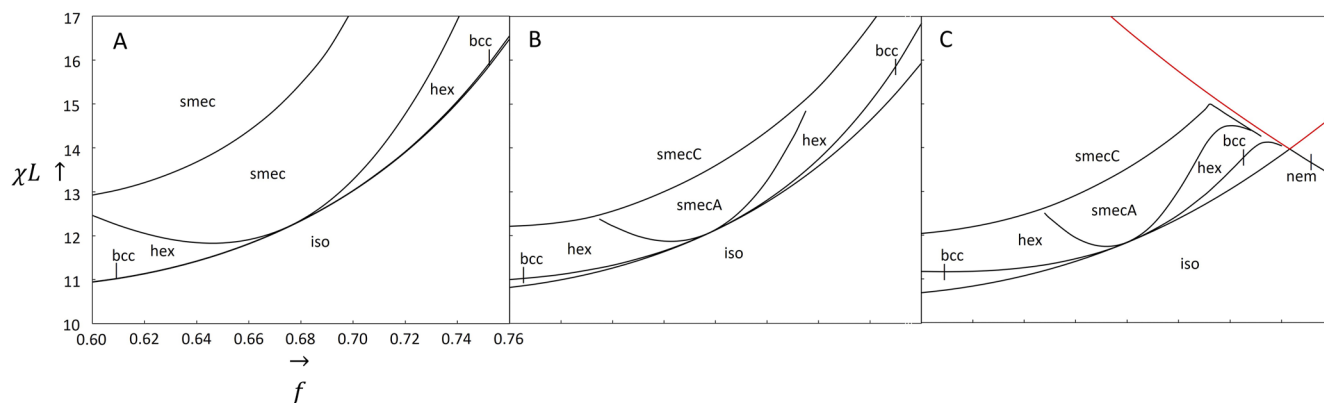

FIG. 3. Phase diagrams of a semi–coil diblock in which $\lambda_A/L = 10^{-1}$; $\lambda_B/L = 10^{-4}$; and $r = 0, 3,$ and 5. In (a), $r = 0$ is chosen; in (b), $r = 3$; and in (c), $r = 5$.

In Fig. 3, the effect of r on the bcc, hexagonal, and smectic-A phase is the same as in Fig. 1, but the smectic-C phase behaves in an opposite way. It moves to a greater χ when decreasing r, and at $r = 0$, it disappears if $f > 0.706$. The orientation θ varies between 8° and 18° in previous system (a), but in system (b), it has a fixed value of 54.7°. When $\theta = 54.7°$, it appears that the alignment of A-blocks in the x-direction perpendicular to the layers is completely arbitrary. This follows from the director η, which is applied in the orientation tensor $\underline{\underline{Q}}^{\alpha}(\underline{x})$ given by Eq. (C1). The director part $\eta^{\alpha}(\underline{x})\eta^{\alpha}(\underline{x}) - \frac{1}{3}\underline{\underline{I}}$ of this tensor is $\eta_x^2 - \frac{1}{3} = \cos^2\theta - \frac{1}{3}$ in component Q_{xx}^{α}. If $\theta = 54.7°$, then $\eta_x^2 - \frac{1}{3} = \cos^2\theta - \frac{1}{3} = 0$ and, consequently, $Q_{xx}^{\alpha} = 0$. The components Q_{xx}^{α}, Q_{yy}^{α}, and Q_{zz}^{α} add up to zero, $Q_{xx}^{\alpha} + Q_{yy}^{\alpha} + Q_{zz}^{\alpha} = 0$, because η^{α} is a unit vector. Hence, if $Q_{xx}^{\alpha} = 0$, then $Q_{yy}^{\alpha} = -Q_{zz}^{\alpha}$, which means that the A-blocks tend to align parallel to the layers. In the middle of an A-rich layer, the A-blocks are aligned at maximum strength in a certain direction for which we choose the y-direction. While we travel in the x-direction to a B-rich layer, the alignment is rotating. In the middle of a B-rich layer, it has rotated to the z-direction at maximum strength again. Therefore, in the smectic-C phase, a spiral-like structure would be formed. However, when we numerically calculate the primary eigenvector $\underline{x}_1 = (\Psi_1, \Upsilon_1^A, \Upsilon_1^B)$, it appears that this vector is always equal to $\underline{x}_1 = (\Psi_1, 0, 0)$. This result is logical because a preferred direction of rotation does not exist, so each spiral is a possible state. This averages out the alignment in the y- and z-direction such that only one state is left, which is a state without alignment. Only the contributions of the secondary eigenvectors may result in a nonzero but negligible alignment. Hence, the smectic-C phase is actually a lamellar phase without alignment when $\theta = 54.7°$. Later on, in this paper, it appears that in system (c), this lamellar phase is also formed and can be explained in the same logical way. In systems (a)–(c), irrespective of the presence of Maier–Saupe interaction, alignment will always occur to form a stable layered structure if $\theta \neq 54.7°$. This is necessary to separate A- and B-blocks sufficiently to increase separation enthalpy. However, alignment reduces entropy. Apparently, this reduction is compensated by the additional enthalpy.

To understand the effect of r observed in Fig. 3, the components $|\Psi_1|$ and $|\Upsilon_1^A|$ in the primary eigenvector $\underline{x}_1 = (\Psi_1, \Upsilon_1^A, \Upsilon_1^B)$ are again investigated in different microphase structures. It appears that the density parameter $|\Psi_1|$ is also ordered according to Eq. (21),

$$|\Psi_{1,smecC}| \geq |\Psi_{1,smecA}| \geq |\Psi_{1,hex}| \geq |\Psi_{1,bcc}|. \tag{27}$$

The orientation strength $|\Upsilon_1^A|$ is ordered by

$$|\Upsilon_{1,smecA}^A| \geq |\Upsilon_{1,hex}^A| \geq |\Upsilon_{1,bcc}^A| \geq |\Upsilon_{1,smecC}^A| = 0, \tag{28}$$

which is different if we look at Eq. (22). In Eq. (22), the smectic-C phase has the strongest orientation, but in Eq. (28), $|\Upsilon_{1,smecC}^A| = 0$ because $\theta = 54.7°$.

Therefore, it has appeared that the influence of r on the density parameter $|\Psi_{1,smecC}|$ is negligible. $|\Psi_{1,smecA}|$, $|\Psi_{1,hex}|$, and $|\Psi_{1,bcc}|$ are lowered when increasing r. The parameter r hardly changes the alignment $|\Upsilon_1^A|$ in each observed microphase. When we look at Fig. 3 and Eq. (27), we conclude that in the neighborhood of the critical point, the Maier–Saupe interaction ω weakens the separation of A- and B-blocks because structures with lower components $|\Psi_1|$ and $|\Upsilon_1^A|$ become more dominant. Above the critical point at a larger

χ, a smectic-C structure is predicted, which has the strongest separation $|\Psi_1|$; see also Eq. (27). The parameter r hardly changes this separation because $|\Upsilon_{1,smecC}^A| = 0$ in Eq. (28). It can only be modified indirectly by the secondary parameter $|x_{10}| = |\Upsilon_{10}^A|$, see also Eq. (23), which is a very weak global alignment and therefore cannot influence $|\Psi_1|$ very much. At a larger r, this secondary parameter becomes stronger. In structures other than the smectic-C phase, $|\Psi_1|$ is weakened when increasing r. Apparently, above the critical point, this reduces the separation enthalpy in these other structures such that melt prefers the smectic-C phase, which becomes possible at a lower χ. Hence, in the neighborhood of the critical point, the Maier–Saupe interaction reduces the separation of A- and B-blocks, but at a larger χ, the contrary effect is observed because of the enhanced preference of a smectic-C phase with a stronger $|\Psi_1|$.

In Fig. 4, six phase diagrams are calculated for system (c). In systems (a) and (b), the alignment Υ_B of the fully flexible B-block is neglected, but in system (c), both alignments Υ_A and Υ_B may not be ignored because both blocks can be considered as semi-flexible. Consequently, the Maier–Saupe parameters ω_{AB} and ω_{BB} have to be included in addition to ω_{AA}. Hence, there are three ratios r_{AA}, r_{AB}, and r_{BB} given by $r_{\alpha\beta} = \frac{\omega_{\alpha\beta}}{\chi}$. In Fig. 4, each ratio is restricted to values 0 or 5. Additionally, $r_{AA} \leq r_{BB}$ so that six combinations of ratios are possible. Combinations for which $r_{AA} > r_{BB}$ can be disregarded because the A- and B-blocks are indistinguishable in a mathematical sense. For each combination, a phase diagram is calculated. In Figs. 4(a)–4(c), $r_{AB} = 0$ is constant and the other parameters r_{AA} and r_{BB} are varied. In Figs. 4(a) and 4(c), these parameters are equal and given by $r_{AA} = r_{BB} = 0$ and $r_{AA} = r_{BB} = 5$, respectively. The unequal combination $r_{AA} = 0$ and $r_{BB} = 5$ is applied in Fig. 4(b). In Figs. 4(d)–4(f), $r_{AB} = 5$ and r_{AA} and r_{BB} are varied in the same way as in Figs. 4(a)–4(c).

Comparing Figs. 4(a) and 4(b), we see that the effect of r_{BB} on the formation of microphase structures close to critical point is similar to the effect of r observed in Fig. 3. The influence of r_{BB} on the smectic-C phase is also similar. When r_{AA} becomes 5, the same similarities can be observed in Fig. 4(c). The phase diagram is asymmetric in Fig. 4(b) because on the right side, the B-block is shorter so that r_{BB} has less influence. The effect of r_{AA} and r_{BB} on the phase formation that occurs in Figs. 4(a)–4(c) also occurs in Figs. 4(d)–4(f). However, parameter r_{AB} changes the phases in exactly the opposite way. Further away from $f = 0.5$, this opposite influence is weaker due to the reduced contact between the A- and B-monomer in the melt. In Fig. 4(d), parameter r_{AB} is dominating the most because it is not counteracted by r_{AA} and r_{BB}. Due to this dominance, only a smectic-A state is possible. In Fig. 4(e), at the left side, the smectic-C, hexagonal, and bcc structures come back because here r_{BB} overcomes the force of r_{AB}. These structures reappear at both sides in Fig. 4(f) because r_{AA} is added, which suppresses r_{AB} at the right side.

The counteracting of r_{AB} on r_{AA} and r_{BB} also appears from Figs. 4(a) and 4(f). In both phase diagrams at $f = 0.5$, the smectic-C phase is predicted at $\chi L = 10.69$, which is not coincidental. In Fig. 4(f), the three parameters are equal to 5, and exactly at $f = 0.5$, the influence of r_{AB} is as strong as the influence of both parameters r_{AA} and r_{BB}. They cancel each other out exactly such that they cannot affect the phase structure any more. Hence, at $f = 0.5$, it does not matter if the three parameters are equal to 5 or any other value, such as 0 in Fig. 4(a).
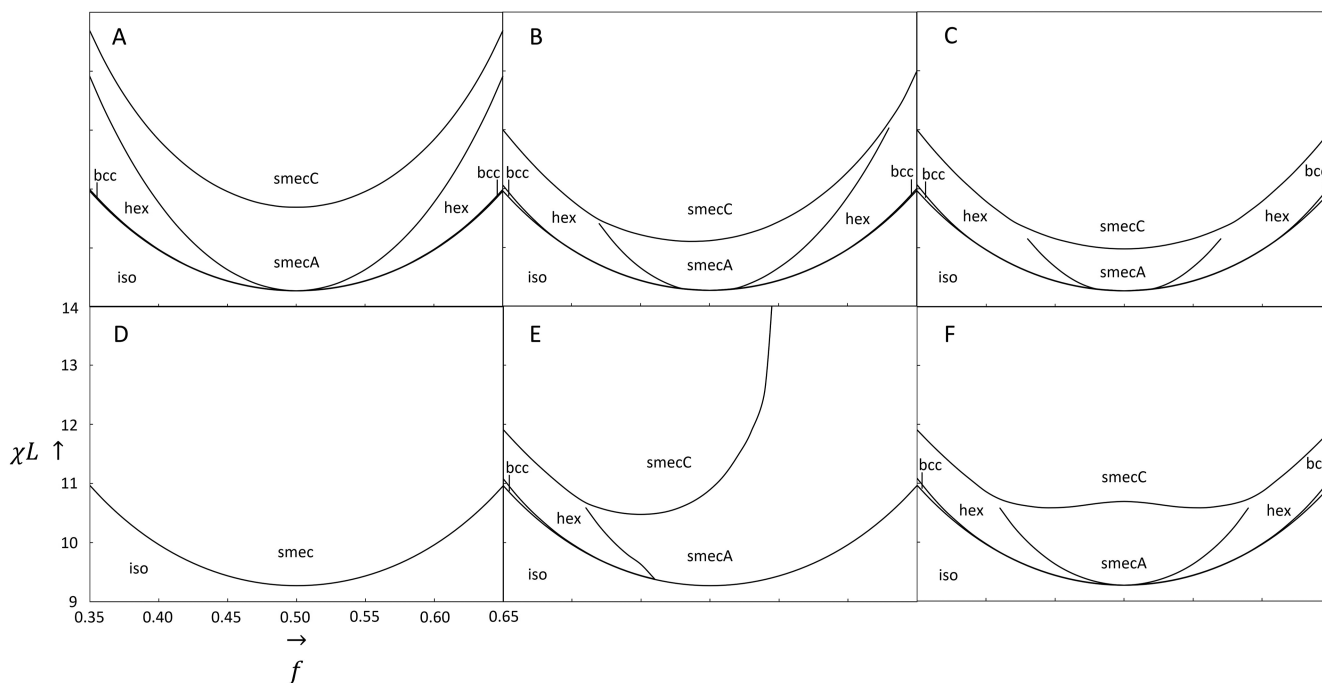
FIG. 4. Phase diagrams of a semi–semi-diblock in which $\lambda_A/L = \lambda_B/L = 10^{-1}$ and r_{AA}, r_{AB}, and $r_{BB} = 0$ or 5. In (a), $r_{AA} = r_{AB} = r_{BB} = 0$ is chosen; in (b), $r_{AA} = r_{AB} = 0$ and $r_{BB} = 5$; in (c), $r_{AA} = r_{BB} = 5$ and $r_{AB} = 0$; in (d), $r_{AA} = r_{BB} = 0$ and $r_{AB} = 5$; in (e), $r_{AA} = 0$ and $r_{AB} = r_{BB} = 5$; and in (f), $r_{AA} = r_{AB} = r_{BB} = 5$.

In Fig. 4, the nematic phase has not appeared. However, by means of numerical calculations, it has been verified that a nematic phase is possible for system (c). When the Maier–Saupe parameters ω_{AA}, ω_{AB}, and ω_{BB} are taken equal, a spinodal ω_s can be derived from the first matrix in Eq. (B5). It appears that ω_s has a minimum at wave number $q_* = 0$ if $\chi < \chi_s$. This spinodal value ω_s is about ten times larger than χ_s in the neighborhood of $f = 0.5$, so here a strong $\omega = \omega_{AA} = \omega_{AB} = \omega_{BB}$ is necessary to induce nematic ordering. This explains why there is no nematic phase in Fig. 4. For combinations other than $\omega_{AA} = \omega_{AB} = \omega_{BB}$, it is very plausible that a nematic phase can also be formed. Additionally, when we look at Figs. 1 and 3, we see that a nematic phase is not missing for systems (a) and (b). It appears in the area in which $\chi < \chi_s$ and $\omega = \omega_{AA} > \omega_s$.

Earlier in this paper, it is explained why in Fig. 3 in the neighborhood of the critical point the smectic-A, hexagonal, and bcc phases become more dominant when increasing r, but at the same time, the smectic-C phase behaves in an opposite way. In Fig. 4, the same behavior is observed when increasing r_{AA} or r_{BB}. Here, the same explanation can be applied. When increasing the other parameter r_{AB}, the opposite behavior occurs, which is quite logical. Furthermore, in the smectic-C phase in Fig. 4, it appears that θ is again 54.7°. Hence, as mentioned earlier, in that case, the primary eigenvector is always $\underline{x}_1 = (\Psi_1, \Upsilon_1^A, \Upsilon_1^B) = (\Psi_1, 0, 0)$ so that this phase is actually a lamellar phase.

In systems (a) and (b), the B-block is fully flexible such that the alignment of the B-blocks can be ignored. When the A-block is also made fully flexible, the system described in Leibler's paper[5] can be reproduced. It appears that the contributions in Eq. (20)

containing alignment tensors reach zero when the stiffness of both blocks is made very small so that it is allowed to exclude these contributions. In this way, the phase diagram is calculated, which is in agreement with Leibler's result in Ref. 5.

At $f = 0.5$ in the phase diagram according to Ref. 5 and in Fig. 4, the A- and B-blocks are indistinguishable in a mathematical sense. Due to this indistinguishability, it is not possible to form a bcc or hexagonal phase. Only a layered structure can be formed whose density and alignment amplitude x_1 of the primary eigenvector, see also Eq. (B10), reach zero as close as possible when χ is lowered to the spinodal χ_s as close as possible. Here, we reach the critical point at which $f = f_c = 0.5$. Such a critical point is also possible in systems (a) and (b) in which the blocks are distinguishable. It is found at $f = 0.68$ in Figs. 1 and 3. At the left of $f = f_c$ just above χ_s, the rod-like or semi-flexible A-block prefers to form spheres in a bcc phase or cylinders in a hexagonal phase. Outside these separated domains with higher density of A-monomers, there is an environment with a higher density of B-monomers. When f increases, the spheres or cylinders are growing in size and getting too large at $f = f_c$ such that at the right of f_c, a reverse phase is formed by B-rich spheres or cylinders in an A-rich environment. At the limit $f = f_c$, both the phase with an A-rich environment and its reverse state with a B-rich environment are possible, which makes the separation of A- and B-blocks impossible for the bcc and hexagonal phase. Again, only a layered structure can be formed because for this structure, a reverse state does not exist. In Figs. 1 and 3, at the critical point, the fully flexible B-block is shorter than the A-block. Due to the flexibility of the B-block, it is apparently easier to form B-rich environment so

that the melt still prefers this state between $f = 0.5$ and $f = f_c = 0.68$. In the reverse state, less chain configurations could be possible in the whole melt.

In Figs. 1, 3, and 4 at or in the neighborhood of $f = f_c$, the smectic-C phase is always found at a larger χ after the smectic-A phase. Apparently, a stronger separation of the A- and B-blocks is possible in the smectic-C phase. This is made clear in Fig. 5 in which A-rich layers are drawn in the smectic-A and smectic-C phase in the left and right part, respectively. In the left part, the A-block is positioned such that the concentration of A-blocks has a maximum value in the middle, but at the same time, this maximum must be as low as possible. This positioning follows from extensive analysis and visualizations of the orientation order-parameter of the A-block in the smectic-A phase. It appears that the A-blocks align stronger in the same directions as the wave vector $\underline{q}$ when the concentration of A-blocks is minimal. At the maximum concentration, they tend to align more in a direction parallel to the layers as we see in the left part of Fig. 5. In the right part, the orientation θ has become nonzero so that the B-block is moved to the B-rich layer. This could increase the separation, which could explain why a smectic-C phase is not favorable in the neighborhood of the critical point. Second, a smectic-A phase is entropically more favorable due to the rotational symmetry with respect to the wave vector $\underline{q}$. This symmetrical property is missing in the smectic-C phase.

When the A- and B-blocks are separated, a not very sharp boundary surface is formed between A-rich and B-rich regions. The total size of this surface depends on the kind of microphase structure. For the total area of the layered structure $A_{layered}$, hexagonal phase A_{hex}, and bcc phase A_{bcc}, the following relation can easily be derived:

$$A_{layered} : A_{hex} : A_{bcc} = 1 : 2 : 3. \quad (29)$$

The larger the size of the boundary surface, the weaker the separation, which could explain the order of phases in the neighborhood of the critical point in Figs. 1, 3, and 4 when χ is increased. Near χ_s, a state with a large boundary is formed because of mixing entropy. Further away from χ_s, the enthalpic contributions of the Flory–Huggins and/or Maier–Saupe interaction increase, which make states with a larger separation more preferable.
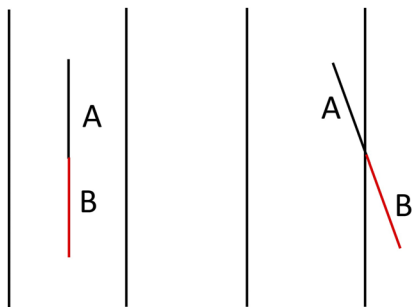

FIG. 5. Orientation of an A-block in the middle of an A-rich layer in the smectic-A and smectic-C phase.

V. CONCLUDING REMARKS

In Sec. III and Appendix A, we develop a general theory of a polydisperse semi-flexible multi-block copolymer melt in which the final form of the Landau free energy has become a power series expansion of density and orientation order-parameters. This general theory is an extension of the theory in Ref. 1 in which the chains are totally flexible. In that case, a possible orientation of chains can be neglected so that the Maier–Saupe interaction does not contribute. Only the Flory–Huggins interaction and density order-parameters are included when we derive the final form of the Landau free energy. However, in our model, an important extension has been realized by making each block semi-flexible by assigning a persistent length using the Bawendi–Freed approach. Due to the stiffness, the orientation of chains may become possible so that the Maier–Saupe interaction and orientation order-parameters have to be included in the derivation of the Landau free energy besides the Flory–Huggins interaction and density order-parameters.

In Appendix B, we show that the final form of the general Landau free energy can be reduced to a much simpler form if the melt only contains diblock copolymers, which are semi-flexible. First, the second order terms are written in the matrix form. After that, the eigenvectors of that matrix are determined, which are used to express the free energy as a function of eigenvectors instead of density and orientation order-parameters. In the ordered state close to the critical point, one eigenvector is dominating, which we call the primary eigenvector. It appears that the Landau free energy can be simplified to power series expansion of only one variable, which is the magnitude of that primary eigenvector. Numerical methods are not necessary to find the minimum. The simplified expression can be applied to both monodisperse and polydisperse diblock copolymers, but for now, we do not consider polydispersity.

Due to the bending stiffness, the orientation order-parameter must also be included in addition to the density order-parameter. This alignment has a space dependent and independent part. In the space dependent part, the director vector has a fixed direction for a layered structure, but for the hexagonal or bcc phase, it is more complicated. In Appendix C, an orientation tensor has been made for these more complex structures, which is a composition of multiple orientation tensors of smectic-A phases with different director vectors. These compositions allow us to also calculate the Landau free energy for the hexagonal or bcc phase using the simplified form in Appendix B.

The theory in Appendixes B and C is used to calculate the phase diagrams for the following monodisperse systems: (a) rod–coil system ($\lambda_A/L_A = 10^2 \gg \lambda_B/L_B = 10^{-4}$); (b) semi–coil system ($\lambda_A/L_A = 10^{-1} \gg \lambda_B/L_B = 10^{-4}$); and (c) semi–semi system ($\lambda_A/L_A = 10^{-1} = \lambda_B/L_B$). In each system, phase diagrams are calculated in which the chain composition and Flory–Huggins interaction strength are varied. The strengths of the Maier–Saupe and Flory–Huggins interaction can be chosen to be proportional to each other using a constant ratio between them. In each phase diagram, a different fixed ratio is applied. The nematic, smectic-A, smectic-C, hexagonal, and bcc structures appear to be possible in systems (a)–(c). In system (a), the Maier–Saupe interaction reduces the separation between the A- and B-blocks everywhere above the spinodal χ_s, but in systems (b) and (c), this is only observed in the neighborhood of the critical point. Further away from the critical

point, the smectic-A phase is converted into a smectic-C phase in systems (a)–(c). In this phase, in system (a), the orientation angle θ varies between $8°$ and $18°$, but in systems (b) and (c), it is fixed at $54.7°$. When $\theta = 54.7°$, it turns out that there is an enlarged microphase separation compared to the bcc, hexagonal, and smectic-A phase. On the other hand, there is hardly alignment such that this smectic-C phase is actually a lamellar structure. In systems (b) and (c), at a stronger Maier–Saupe interaction, this lamellar structure moves closer to χ_s so that here the separation between the A- and B-blocks is not reduced, but stimulated. In system (a), we see exactly the opposite effect. In systems (a) and (b), the alignment of fully flexible B-blocks is neglected, but in system (c), this alignment cannot be ignored. Consequently, instead of only one Maier–Saupe parameter ω_{AA}, three parameters ω_{AA}, ω_{AB}, and ω_{BB} are taken into account. Earlier, we explained the effect of the Maier–Saupe interaction on the formation of microphase structures in system (b). It appears that in system (c), ω_{AA} and ω_{BB} have the same effect, but ω_{AB} does exactly the opposite.

This paper contains three new aspects, which have not yet been applied or investigated in other papers before. First, the Bawendi–Freed approach is applied to model semi-flexibility. This approach enables us to derive explicit expressions of the single-chain correlation functions such that the explicit expression of the Landau free energy can also be obtained. Second, the complete phase diagram has been calculated for a system of diblocks in which the block lengths are fixed, but the stiffness of each block can be chosen arbitrary. Other papers are restricted to spinodal calculations, or the complete phase diagram has been calculated for more simplified systems. Third, a space dependent orientation order-parameter is described in microphase structures, such as the hexagonal phase. In other papers, this was not necessary because these were restricted to spinodal calculations or the space dependent orientation order-parameter was not included in the calculation of the complete phase diagram.

SUPPLEMENTARY MATERIAL

See the supplementary material for more details on the derivation of the Landau free energy (Secs. II and III) and single-chain correlation functions (Secs. I and IV).

AUTHOR DECLARATIONS

Conflict of Interest

The authors have no conflicts to disclose.

Author Contributions

P. M. Jager: Investigation (equal); Methodology (supporting); Writing – original draft (lead). **W. J. Briels**: Investigation (equal); Methodology (equal); Writing – review & editing (equal). **J. J. M. Slot**: Conceptualization (lead); Investigation (equal); Methodology (lead); Supervision (equal); Writing – review & editing (equal).

DATA AVAILABILITY

The data that support the findings of this study are available from the corresponding author upon reasonable request.

APPENDIX A: DERIVATION OF THE LANDAU FREE ENERGY

In this appendix, the Landau free energy given by Eq. (20) is derived. The starting point of the derivation is the partition function Z, i.e., the sum of the *Boltzmann weights* over all allowed states of the system. The set of all allowed states furnishes the so-called *state-space* or *configuration-space* Γ of the system, which in this case is given by

$$\Gamma \equiv \{\{\underline{R}_m^s, \underline{u}_m^s\}_{sm} \mid \underline{u}_m^s \equiv \dot{\underline{R}}_m^s, \quad \forall \; m,s \quad \& \quad \hat{\rho}(\underline{x}) = 1, \quad \forall \underline{x} \in V\}. \tag{A1}$$

As we are ultimately only interested in differences in free energy between possible inhomogeneous and/or anisotropic phases of the system, all combinatorial terms will be left out of this partition function since they only lead to constant terms in the free energy. With this in mind, Z can be written as

$$Z \equiv \prod_{sm} \int d^3\widetilde{U}_m^s \int d^3 U_m^s G(\{\underline{U}_m^s, L_s\} \mid \{\underline{\widetilde{U}}_m^s, 0\}), \tag{A2}$$

where the *orientational Green's function* $G(\{\underline{U}_m^s, L_s\} \mid \{\underline{\widetilde{U}}_m^s, 0\})$ is defined by

$$G \equiv \prod_{sm} \int D\underline{R}_m^s \int_{(0,\underline{\widetilde{U}}_m^s)}^{(L_s,\underline{U}_m^s)} D\underline{u}_m^s \; \delta\left[\underline{R}_m^s - \int dl \; \underline{u}_m^s(l)\right]$$
$$\times \delta[1 - \hat{\rho}] \; e^{-(\hat{H}_0 + \hat{W})}, \tag{A3}$$

which gives the probability that each chain has a certain initial and final orientation. In this coarse-grained description, incompressibility, which is due to interactions at the molecular level, has to be explicitly accounted for via the delta function $\delta[1 - \hat{\rho}]$. This partition function will be transformed in four steps into a form that is more amendable for further analysis. The first step involves a formal shift of the state-variable dependence of $e^{-\hat{W}}$ in (A3). This is done by introducing the following two *functional decompositions of the identity* into G:

$$\prod_{\mu}' \int D\psi^\mu \; \delta[\psi^\mu - \hat{\psi}^\mu] = 1 \tag{A4}$$

and

$$\prod_{\nu} \int D\underline{\underline{Q}}^\nu \; \delta[\underline{\underline{Q}}^\nu - \hat{\underline{\underline{Q}}}^\nu] = \underline{I}, \tag{A5}$$

which yield

$$G = \prod_\mu{}' \int D\psi^\mu \prod_\nu \int D\underline{\underline{Q}}^\nu \, e^{-W} \prod_{sm} \int D\underline{R}^s_m \int_{(0,\widetilde{\underline{U}}^s_m)}^{(L_s,\underline{U}^s_m)}$$

$$\times \, D\underline{u}^s_m \, e^{-\hat{H}_0} \, \delta\left[\underline{R}^s_m - \int dl \, \underline{u}^s_m(l)\right] \delta[1-\hat{\rho}]\prod_\lambda{}'$$

$$\times \prod_\eta \delta\left[\psi^\lambda - \hat{\psi}^\lambda\right] \delta\left[\underline{\underline{Q}}^\eta - \underline{\underline{\hat{Q}}}^\eta\right]. \tag{A6}$$

The elements Q^ν_{ij} and Q^ν_{ji} of the tensor $\underline{\underline{Q}}^\nu$ in which $i \neq j$ are identical, but in Eq. (A6), they are treated as independent parameters. At a certain point, this would obstruct the further derivation of the Landau free energy. This happens when we solve Eqs. (II.2) and (II.3) in Sec. II of the supplementary material iteratively because then the matrix $A^{\bar{a}\bar{b}}$ would not be invertible. In this matrix, the rows and columns in which $ij = xy, yz$, and xz would be identical to the rows and columns with reversed indices $ij = yx, zy$, and zx. Such a matrix is not invertible. Therefore, in the functional integral in Eq. (A6), only the elements Q^ν_{ij} with unique pairs xx, yy, zz, xy, yz, and xz may occur if we want to derive the desired expression of the Landau free

energy. In the rest of the derivation, we will ignore the other pairs yx, zy, and zx. In the interaction energy W given by Eq. (13), the terms containing elements Q^ν_{ij} with $i \neq j$ are counted twice.[64]

The second step involves the substitution of the following *functional spectral representations* for the last $2M$ "delta-functions" in the above expression, i.e.,

$$\delta[1-\hat{\rho}] \equiv \int Dh^0 \, \exp\left(i\int_V d^3x \, h^0(\underline{x}) \, \{1-\hat{\rho}(\underline{x})\}\right), \tag{A7}$$

$$\delta\left[\psi^\lambda - \hat{\psi}^\lambda\right] \equiv \int Dh^\lambda \, \exp\left(i\int_V d^3x \, h^\lambda(\underline{x}) \, \{\psi^\lambda(\underline{x}) - \hat{\psi}^\lambda(\underline{x})\}\right)$$
$$(\lambda = 1,\ldots,M-1), \tag{A8}$$

$$\delta\left[\underline{\underline{Q}}^\eta - \underline{\underline{\hat{Q}}}^\eta\right] \equiv \int D\underline{\underline{K}}^\eta \, \exp\left(i\int_V d^3x \, \underline{\underline{K}}^\eta(\underline{x}) : \{\underline{\underline{Q}}^\eta(\underline{x}) - \underline{\underline{\hat{Q}}}^\eta(\underline{x})\}\right)$$
$$(\eta = 1,\ldots,M), \tag{A9}$$

resulting in

$$G = \prod_\mu{}' \int D\psi^\mu \prod_\nu \int D\underline{\underline{Q}}^\nu \, e^{-W} \int Dh^0 \prod_\lambda{}' \int Dh^\lambda \prod_\eta \int D\underline{\underline{K}}^\eta$$

$$\times \exp\left(i\int_V d^3x \left\{ h^0(\underline{x}) + \sum_\alpha{}' h^\alpha(\underline{x}) \, \psi^\alpha(\underline{x}) + \sum_\beta \underline{\underline{K}}^\beta(\underline{x}) : \underline{\underline{Q}}^\beta(\underline{x}) \right\}\right)$$

$$\times \prod_{sm} \int D\underline{R}^s_m \int_{(0,\widetilde{\underline{U}}^s_m)}^{(L_s,\underline{U}^s_m)} D\underline{u}^s_m \, e^{-\hat{H}_0} \, \delta\left[\underline{R}^s_m - \int dl \, \underline{u}^s_m(l)\right]$$

$$\times \exp\left(- \, i\int_V d^3x \left\{ h^0(\underline{x}) \, \hat{\rho}(\underline{x}) + \sum_\alpha{}' h^\alpha(\underline{x}) \, \hat{\psi}^\alpha(\underline{x}) + \sum_\beta \underline{\underline{K}}^\beta(\underline{x}) : \underline{\underline{\hat{Q}}}^\beta(\underline{x}) \right\}\right). \tag{A10}$$

In the third step, the auxiliary integration fields $h^0(\underline{x})$, $h^1(\underline{x}),\ldots,h^{M-1}(\underline{x})$ are transformed to new fields $J^1(\underline{x}),\ldots,J^M(\underline{x})$, defined in the following way:

$$J^\alpha(\underline{x}) \equiv h^\alpha(\underline{x}) + h^0(\underline{x}) \quad (\alpha = 1,\ldots,M-1), \quad J^M(\underline{x}) \equiv h^0(\underline{x}). \tag{A11}$$

Using this isometric transformation and (3) and (7)–(9), it is easily verified that the following identities hold:

$$h^0(\underline{x})\hat{\rho}(\underline{x}) + \sum_\alpha{}' h^\alpha(\underline{x}) \, \hat{\psi}^\alpha(\underline{x})$$
$$= J^M(\underline{x}) + \sum_\alpha{}' J^\alpha(\underline{x}) \, \hat{\rho}^\alpha(\underline{x}) - \sum_\alpha f^\alpha \, J^\alpha(\underline{x}), \tag{A12a}$$

$$h^0(\underline{x}) + \sum_\alpha{}' h^\alpha(\underline{x}) \, \psi^\alpha(\underline{x}) = J^M(\underline{x}) + \sum_\alpha J^\alpha(\underline{x}) \, \psi^\alpha(\underline{x}), \tag{A12b}$$

and so by combining (A10) with (A2), Z can be written as

$$Z = \prod_\mu{}' \int D\psi^\mu \prod_\nu \int D\underline{\underline{Q}}^\nu \, e^{-W} \prod_\lambda \int DJ^\lambda \prod_\eta \int D\underline{\underline{K}}^\eta$$

$$\times \exp\left(i\int_V d^3x \left\{ \sum_\alpha J^\alpha(\underline{x}) \, [\psi^\alpha(\underline{x}) + f^\alpha] + \sum_\beta \underline{\underline{K}}^\beta(\underline{x}) : \right.\right.$$

$$\times \left. \left[\underline{\underline{Q}}^\beta(\underline{x}) + \frac{1}{3}\rho^\beta(\underline{x}) \, \underline{\underline{I}} \right]\right\}\right) \left\langle \exp\left(- \, i\int_V d^3x \left\{ \sum_\alpha J^\alpha(\underline{x}) \, \hat{\rho}^\alpha(\underline{x}) \right.\right.\right.$$

$$\left.\left.\left. + \sum_\beta \underline{\underline{K}}^\beta(\underline{x}) : \underline{\underline{\hat{Q}}}^\beta(\underline{x}) \right\}\right)\right\rangle_0. \tag{A13}$$

In this expression, $\langle\cdots\rangle_0$ denotes an average with respect to the *unperturbed ensemble of chain conformations* defined by $\hat{H}_0$, i.e.,

$$\langle \hat{A} \rangle_0 \equiv \prod_{sm} \int d^3\widetilde{U}^s_m \int d^3 U^s_m \int D\underline{R}^s_m \int_{(0,\widetilde{\underline{U}}^s_m)}^{(L_s,\underline{U}^s_m)} D\underline{u}^s_m \, e^{-\hat{H}_0}$$

$$\times \delta\left[\underline{R}^s_m - \int dl \, \underline{u}^s_m(l)\right] \hat{A}, \tag{A14}$$

where $\hat{H}_0$ is the *unperturbed Hamiltonian* according to the Bawendi–Freed approach, which has earlier been defined in Sec. III in Eq. (17). In Eq. (A14), the functional integrations over $\{\underline{R}^s_m\}$ and $\{\underline{u}^s_m\}$ are defined in such a way that $\langle 1 \rangle_0 \equiv 1$. The last step in the transformation of Z boils down to rewriting the integrand of (A13) using the fields $\tilde{J}^1(\underline{x}), \ldots, \tilde{J}^M(\underline{x})$ in the spirit of Ref. 65,

$$\tilde{J}^\alpha(\underline{x}) \equiv J^\alpha(\underline{x}) - \frac{1}{V} \int_V d^3 y \, J^\alpha(\underline{y}) \quad (\alpha = 1, \ldots, M). \tag{A15}$$

It is easy to see that the use of these new fields in conjunction with (5) will eliminate the terms in (A13) involving f^α. Thus, we finally end up with

$$Z = \prod_\mu' \int D\psi^\mu \prod_\nu \int D\underline{\underline{Q}}^\nu \, e^{-W} \prod_\lambda \int DJ^\lambda \prod_\eta \int D\underline{\underline{K}}^\eta$$
$$\times \exp\left(i \int_V d^3 x \left\{ \sum_\alpha \tilde{J}^\alpha(\underline{x}) \, \psi^\alpha(\underline{x}) + \sum_\beta \underline{\underline{K}}^\beta(\underline{x}) : \underline{\underline{Q}}^\beta(\underline{x}) \right\} + \Lambda \right), \tag{A16}$$

with Λ defined by

$$\Lambda \equiv \ln \left\langle \exp\left(-i \int_V d^3 x \left\{ \sum_\alpha \tilde{J}^\alpha(\underline{x}) \, \hat{\rho}^\alpha(\underline{x}) + \sum_\beta \underline{\underline{K}}^\beta(\underline{x}) : \underline{\underline{\hat{Q}}}^\beta(\underline{x}) \right\} \right) \right\rangle_0. \tag{A17}$$

By Fourier-transforming all the integrals involving the ψ, Q, J, and $\underline{K}$ fields and making use of the fact that according to the definition of $\tilde{\chi}_{\alpha\beta}$ [see Eq. (15)] $\tilde{\chi}_{MM} \equiv 0$, the partition function Z (A16) can be written as

$$Z \equiv \prod_c' \prod_{\bar{d}} \int D\Psi^c \int D\Upsilon^{\bar{d}}$$
$$\times \exp\left(V \left\{ \tilde{\chi}_{ab} \Psi^a \Psi^b + \frac{1}{2} \omega_{\bar{a}\bar{b}} \Upsilon^{\bar{a}} \Upsilon^{\bar{b}} \right\} \right) \widetilde{Z}[\underline{\Psi}, \overline{\Upsilon}] \tag{A18}$$

with $\tilde{\chi}_{ab} \equiv \tilde{\chi}_{\alpha\beta} \, \delta(\underline{q}_1 + \underline{q}_2)$, $\omega_{\bar{a}\bar{b}} \equiv \omega_{\alpha\beta} |2\delta_{ii'}\delta_{jj'} - \delta_{ij}\delta_{i'j'}| \, \delta(\underline{q}_1 + \underline{q}_2)$, $\Psi^a \equiv \frac{\psi^\alpha(-\underline{q})}{V}$, $\Upsilon^{\bar{a}} \equiv \frac{Q^\alpha_{ij}(-\underline{q})}{V}$, and

$$\widetilde{Z}[\underline{\Psi}, \overline{\Upsilon}] \equiv \prod_g \prod_{\bar{h}} \int Dv_g \int Dw_{\bar{h}}$$
$$\times \exp\left(V \left\{ i \left[v_a \Psi^a + w_{\bar{a}} \Upsilon^{\bar{a}} \right] + \frac{\Lambda[\underline{v}, \overline{w}]}{V} \right\} \right), \tag{A19}$$

where $v_a \equiv \frac{J^\alpha(\underline{q})}{V}$, $w_{\bar{a}} \equiv \frac{K^\alpha_{ij}(\underline{q})}{V}$, $\underline{\Psi} \equiv \{\Psi^a\}_a$, and $\overline{\Upsilon} \equiv \{\Upsilon^{\bar{a}}\}_{\bar{a}}$.

In (A18) and (A19), we use the *composite labels* $a \equiv (\underline{q}_1 \neq \underline{0}, \alpha)$, $b \equiv (\underline{q}_2 \neq \underline{0}, \beta)$, etc. and $\bar{a} \equiv (\underline{q}_1, ij, \alpha)$, $\bar{b} \equiv (\underline{q}_2, i'j', \beta)$, etc. in which the pairs ij and $i'j'$ are one of the six unique pairs xx, yy, zz, xy, xz, and yz. Furthermore, we see that each composite label a, b, $\bar{a}$, or $\bar{b}$ in a subscript matches with a composite label in a superscript. In such a match, the Einstein summation convention is applied. More details

about the derivation of Eqs. (A18) and (A19) from Eq. (A16) can be found in Sec. III of the supplementary material.

For large values of the system's volume V, $\widetilde{Z}[\underline{\Psi}, \overline{\Upsilon}]$ can be evaluated with the well-known *saddle-point method*, i.e., approximating $\widetilde{Z}[\underline{\Psi}, \overline{\Upsilon}]$ by

$$\widetilde{Z}[\underline{\Psi}, \overline{\Upsilon}] \simeq e^{V \, \Phi[\underline{\Psi}, \overline{\Upsilon}]}, \tag{A20}$$

where $\Phi[\underline{\Psi}, \overline{\Upsilon}]$ is the stationary value of $i \left[v_a \Psi^a + w_{\bar{a}} \Upsilon^{\bar{a}} \right] + \frac{\Lambda[\underline{v}, \overline{w}]}{V}$ with respect to the set of v's and w's for which its absolute value is the smallest. This stationary point is a solution of the following set of equations:

$$i\Psi^a = A^{ab} \, v_b + A^{a\bar{b}} \, w_{\bar{b}} - \frac{i}{2} \, B^{abc} \, v_b v_c - i \, B^{a\bar{b}c} \, w_{\bar{b}} v_c - \frac{i}{2} \, B^{a\bar{b}\bar{c}} \, w_{\bar{b}} w_{\bar{c}}$$
$$- \frac{1}{6} \, C^{abcd} \, v_b v_c v_d - \frac{1}{2} \, C^{a\bar{b}cd} \, w_{\bar{b}} v_c v_d - \frac{1}{2} \, C^{a\bar{b}\bar{c}d} \, w_{\bar{b}} w_{\bar{c}} v_d$$
$$- \frac{1}{6} \, C^{a\bar{b}\bar{c}\bar{d}} \, w_{\bar{b}} w_{\bar{c}} w_{\bar{d}}, \quad \forall a, \tag{A21}$$

and

$$i \, \Upsilon^{\bar{a}} = A^{\bar{a}\bar{b}} \, w_{\bar{b}} + A^{\bar{a}b} \, v_b - \frac{i}{2} \, B^{\bar{a}bc} \, v_b v_c - i \, B^{\bar{a}\bar{b}c} w_{\bar{b}} v_c - \frac{i}{2} \, B^{\bar{a}\bar{b}\bar{c}} \, w_{\bar{b}} w_{\bar{c}}$$
$$- \frac{1}{6} \, C^{\bar{a}bcd} \, v_b v_c v_d - \frac{1}{2} \, C^{\bar{a}\bar{b}cd} \, w_{\bar{b}} v_c v_d - \frac{1}{2} \, C^{\bar{a}\bar{b}\bar{c}d} \, w_{\bar{b}} w_{\bar{c}} v_d$$
$$- \frac{1}{6} \, C^{\bar{a}\bar{b}\bar{c}\bar{d}} \, w_{\bar{b}} w_{\bar{c}} w_{\bar{d}}, \quad \forall \bar{a}. \tag{A22}$$

In Eqs. (A21) and (A22), A's, B's, and C's are second, third, and fourth order single-chain correlation functions, respectively. These correlation functions are introduced in Sec. III of the supplementary material and calculated in Appendix B. As we ultimately want to arrive at a Landau free energy as an expansion up-to fourth order in the Ψ^a—and the $\Upsilon^{\bar{a}}$ fields—we only need to solve these last two vector-equations iteratively for v_a and $w_{\bar{a}}$ up-to third order in Ψ's and Υ's. This iterative solution can be found in Sec. II of the supplementary material and is substituted into $i \left[v_a \Psi^a + w_{\bar{a}} \Upsilon^{\bar{a}} \right] + \frac{\Lambda[\underline{v}, \overline{w}]}{V}$ such that we obtain $\Phi[\underline{\Psi}, \overline{\Upsilon}]$ and, hence, the partition function,

$$Z \simeq \prod_c' \prod_{\bar{d}} \int D\Psi^c \int D\Upsilon^{\bar{d}}$$
$$\times \exp\left(V \left\{ \tilde{\chi}_{ab} \Psi^a \Psi^b + \frac{1}{2} \omega_{\bar{a}\bar{b}} \Upsilon^{\bar{a}} \Upsilon^{\bar{b}} + \Phi[\underline{\Psi}, \overline{\Upsilon}] \right\} \right). \tag{A23}$$

The Landau free energy, that is the free energy of the system within the *mean field approximation*, can be obtained by again applying the saddle-point method, but now to approximately evaluate this last set of functional integrals. If we write the result as

$$Z \simeq e^{-F_L}, \tag{A24}$$

then this Landau free energy F_L (in units of $k_B T$) is given by

10 April 2024 11:34:15

$$\frac{F_L}{V} = \min_{\underline{\Psi},\underline{\Upsilon}} \left\{ (\Gamma_{ab}^{(2)} - \widetilde{\chi}_{ab})\Psi^a\Psi^b + 2\Gamma_{a\overline{b}}^{(2)}\Psi^a\Upsilon^{\overline{b}} + \left(\Gamma_{\overline{a}\overline{b}}^{(2)} - \frac{1}{2}\omega_{\overline{a}\overline{b}}\right)\Upsilon^{\overline{a}}\Upsilon^{\overline{b}} \right.$$

$$- \frac{1}{3}\omega_{ab}\Upsilon^{a,ij}\delta_{ij}(\Psi^b + f^b) + \Gamma_{abc}^{(3)}\Psi^a\Psi^b\Psi^c + 3\Gamma_{ab\overline{c}}^{(3)}\Psi^a\Psi^b\Upsilon^{\overline{c}}$$

$$+ 3\Gamma_{a\overline{b}\overline{c}}^{(3)}\Psi^a\Upsilon^{\overline{b}}\Upsilon^{\overline{c}} + \Gamma_{\overline{a}\overline{b}\overline{c}}^{(3)}\Upsilon^{\overline{a}}\Upsilon^{\overline{b}}\Upsilon^{\overline{c}} + \Gamma_{abcd}^{(4)}\Psi^a\Psi^b\Psi^c\Psi^d$$

$$+ 4\Gamma_{abc\overline{d}}^{(4)}\Psi^a\Psi^b\Psi^c\Upsilon^{\overline{d}} + 6\Gamma_{ab\overline{c}\overline{d}}^{(4)}\Psi^a\Psi^b\Upsilon^{\overline{c}}\Upsilon^{\overline{d}} + 4\Gamma_{a\overline{b}\overline{c}\overline{d}}^{(4)}\Psi^a\Upsilon^{\overline{b}}\Upsilon^{\overline{c}}\Upsilon^{\overline{d}}$$

$$\left. + \Gamma_{\overline{a}\overline{b}\overline{c}\overline{d}}^{(4)}\Upsilon^{\overline{a}}\Upsilon^{\overline{b}}\Upsilon^{\overline{c}}\Upsilon^{\overline{d}} \right\}. \tag{A25}$$

The coefficient functions (Γ's) in this expression are called *vertices*, which follow from applying the iterative solution of Eqs. (A21) and (A22) to the partition function (A23); see also Sec. II of the supplementary material for more details. In this way, the vertices only depend on the single-chain correlation functions as mentioned earlier.[66–81]

APPENDIX B: APPLICATION OF THE GENERAL THEORY TO A MELT OF MONODISPERSE SEMI-FLEXIBLE DIBLOCK COPOLYMERS

In Sec. III and Appendix A, we develop a general theory of a polydisperse semi-flexible multi-block copolymer melt in which the final form of the Landau free energy has become a power series expansion of density and orientation order-parameters. In this appendix, we show that the final form of the general Landau free energy can be reduced to a much simpler form if the melt only contains diblock copolymers, which are semi-flexible. Numerical methods are not necessary to find the minimum. The simplified expression can be applied to both monodisperse and polydisperse diblock copolymers, but for now, we do not consider polydispersity. In Appendix C, an orientation tensor has been created for a layered structure and more complex structures in which the director vector does not have a fixed direction.

Near the critical point at which the disordered state is just converted into an ordered structure, the first harmonics approximation according to Ref. 8 can be applied to the Fourier transform of the density and orientation order-parameter denoted by Ψ^a and $\Upsilon^{\overline{a}}$, respectively,

$$\Psi^a = \Psi^A(\underline{q}) = -\Psi^B(\underline{q}) = \Psi(\underline{q}) = \Psi \sum_{\underline{q}'\in H} \exp(i\varphi_{\underline{q}'})\delta(\underline{q} - \underline{q}') \tag{B1}$$

and

$$\Upsilon^{\overline{a}} = \Upsilon_\alpha^{\mu\nu}(\underline{q}) = \Upsilon_\alpha\left(\eta_\alpha^\mu\eta_\alpha^\nu - \frac{1}{3}\delta^{\mu\nu}\right)\sum_{\underline{q}'\in H}\exp(i\varphi_{\underline{q}'})\delta(\underline{q} - \underline{q}')$$

$$+ \Upsilon_\alpha^0\left(\eta_\alpha^\mu\eta_\alpha^\nu - \frac{1}{3}\delta^{\mu\nu}\right)\delta(\underline{q}). \tag{B2}$$

The summation over the wave vectors $\underline{q}'$ is limited over a set $H = \{\pm\underline{q}_1, \pm\underline{q}_2, \ldots\}$ in which all wave vectors have the same fixed magnitude q_*. This set H defines the symmetry properties and wavelength of a phase structure. The magnitude q_* follows from the spinodal expression given by Eq. (B9), which is minimized with respect to the magnitude q_*. In addition to a space dependent alignment, Eq. (B2) contains a second term in which $\underline{q}$ is the null vector. In $\Upsilon^{\overline{a}}$, the vector η_α^μ is the director vector with length 1 along which blocks of kind α may align in a certain degree. We exclude the possibility that the A- and B-blocks may align in different directions if the persistent length is nonzero everywhere in the chain. If the alignment would differ, each diblock must be curved on average, which takes too much energy according to free Hamiltonian given by Eq. (I.2) in Sec. I of the supplementary material in which it is allowed to replace the constant λ by $\lambda(l)$. Consequently, in Eq. (B2), there is only one director η^μ instead of two different directors η_A^μ and η_B^μ.

In Eq. (B2), this director η^μ has a fixed direction so that the alignment tensor can only be used for the nematic phase and layered structures. For the bcc and hexagonal phase, we need a director with a variable direction. This problem is solved in Appendix C in which the alignment tensor of these phases become compositions of multiple smectic-A phases,

$$\underline{\underline{Q}}_{hex}^\alpha(\underline{q}) = \frac{1}{3}\sum_{m=1}^{3}\underline{\underline{Q}}_{smecA}^\alpha(\underline{q}, \underline{\eta}_m) \tag{B3}$$

and

$$\underline{\underline{Q}}_{bcc}^\alpha(\underline{q}) = \frac{1}{6}\sum_{m=1}^{6}\underline{\underline{Q}}_{smecA}^\alpha(\underline{q}, \underline{\eta}_m). \tag{B4}$$

Inserting Eqs. (B1) and (B2) in the second order terms of the final form of the Landau free energy given by Eq. (20) yields the matrix form

$$\frac{F_L^{(2)}}{V} = \begin{bmatrix} \Psi & \Upsilon_A & \Upsilon_B \end{bmatrix}\begin{bmatrix} \widetilde{\Gamma}^{(2)} - \chi & \widetilde{\Gamma}_A^{(2)} & \widetilde{\Gamma}_B^{(2)} \\ \widetilde{\Gamma}_A^{(2)} & \widetilde{\Gamma}_{AA}^{(2)} - \frac{1}{3}\omega_{AA} & \widetilde{\Gamma}_{AB}^{(2)} - \frac{1}{3}\omega_{AB} \\ \widetilde{\Gamma}_B^{(2)} & \widetilde{\Gamma}_{AB}^{(2)} - \frac{1}{3}\omega_{AB} & \widetilde{\Gamma}_{BB}^{(2)} - \frac{1}{3}\omega_{BB} \end{bmatrix}\begin{bmatrix} \Psi \\ \Upsilon_A \\ \Upsilon_B \end{bmatrix} + \begin{bmatrix} \Upsilon_A^0 & \Upsilon_B^0 \end{bmatrix}\begin{bmatrix} \widetilde{\Gamma}_{AA,00}^{(2)} - \frac{1}{3}\omega_{AA} & \widetilde{\Gamma}_{AB,00}^{(2)} - \frac{1}{3}\omega_{AB} \\ \widetilde{\Gamma}_{AB,00}^{(2)} - \frac{1}{3}\omega_{AB} & \widetilde{\Gamma}_{BB,00}^{(2)} - \frac{1}{3}\omega_{BB} \end{bmatrix}\begin{bmatrix} \Upsilon_A^0 \\ \Upsilon_B^0 \end{bmatrix}, \tag{B5}$$

in which the notations

$$\widetilde{\Gamma}^{(2)} = \Gamma_{ab}^{(2)}S^aS^b, \quad \widetilde{\Gamma}_\alpha^{(2)} = \Gamma_{a\overline{b}}^{(2)}S^a d_\alpha^{\overline{b}},$$

$$\widetilde{\Gamma}_{\alpha\beta}^{(2)} = \Gamma_{\overline{a}\overline{b}}^{(2)} d_\alpha^{\overline{a}} d_\beta^{\overline{b}} \text{ and } \widetilde{\Gamma}_{\alpha\beta,00}^{(2)} = \Gamma_{\overline{a}\overline{b}}^{(2)} d_{\alpha,0}^{\overline{a}} d_{\beta,0}^{\overline{b}}, \tag{B6}$$

$$S^a \equiv (1 - 2\delta_{\alpha B}) \exp(i\varphi_{\underline{q}}) = \pm \exp(i\varphi_{\underline{q}}) \text{ and } a = \underline{q}, \alpha, \qquad (B7)$$

and

$$d_\alpha^{\overline{b}} = d_{\alpha,0}^{\overline{b}} \equiv \left(\eta_\beta^{\mu_2} \eta_\beta^{\nu_2} - \frac{1}{3}\delta^{\mu_2 \nu_2} \right) \exp(i\varphi_{\underline{q}})\delta_{\alpha\beta},$$

and

$$\overline{b} = \underline{q}, \beta, \mu_2 \nu_2 \qquad (B8)$$

are applied. Because of the symmetry, the same matrix form according to Eq. (B5) can be obtained when we apply Eqs. (B3) or (B4) instead of Eq. (B2) in the second order terms of Eq. (20).

The three-dimensional symmetric matrix in the first term in Eq. (B5) has three eigenvalues λ_1, λ_2, and λ_3 ordered by $\lambda_1 \leq \lambda_2 \leq \lambda_3$, which cannot be complex numbers due to the symmetry of the matrix. In the disordered state, all eigenvalues must be positive, but near the critical point, when it is just converted into an ordered state, at least one eigenvalue λ_1 is just below zero. Here, $\chi > \chi_s(q_*)$ or $\omega_{\alpha\beta} > \omega_{\alpha\beta,s}(q_*)$ and $q_* > 0$ for both spinodals χ_s and $\omega_{\alpha\beta,s}$. In the same way, the two real eigenvalues $\lambda_{10}, \lambda_{20}$ ordered by $\lambda_{10} \leq \lambda_{20}$ belong to the two-dimensional symmetric matrix in the second term in Eq. (B5) in which $q_* = 0$. In the disordered state, $\lambda_{20} \geq \lambda_{10} > 0$, but if $\omega_{\alpha\beta} > \omega_{\alpha\beta,s}$, then at least $\lambda_{10} < 0$. If $\chi = \chi_s$, then $\lambda_1 = 0$ and, consequently, the determinant of the matrix in the first term of Eq. (B5) is also zero from which it follows that

$$\chi_s = \min_{q_*} \left\{ \widetilde{\Gamma}^{(2)} - \frac{(\widetilde{\Gamma}_B^{(2)})^2 \left(\widetilde{\Gamma}_{AA}^{(2)} - \frac{1}{3}\omega_{AA} \right) + (\widetilde{\Gamma}_A^{(2)})^2 \left(\widetilde{\Gamma}_{BB}^{(2)} - \frac{1}{3}\omega_{BB} \right) - 2\widetilde{\Gamma}_A^{(2)}\widetilde{\Gamma}_B^{(2)} \left(\widetilde{\Gamma}_{AB}^{(2)} - \frac{1}{3}\omega_{AB} \right)}{\left(\widetilde{\Gamma}_{AA}^{(2)} - \frac{1}{3}\omega_{AA} \right)\left(\widetilde{\Gamma}_{BB}^{(2)} - \frac{1}{3}\omega_{BB} \right) - \left(\widetilde{\Gamma}_{AB}^{(2)} - \frac{1}{3}\omega_{AB} \right)^2} \right\}. \qquad (B9)$$

This expression of χ_s can also be used to calculate the spinodals $\omega_{\alpha\beta,s}(q_*)$ in which the wavenumber q_* is the same as in $\chi_s = \chi_s(q_*)$. The spinodal $\omega_{\alpha\beta,s}(q_* = 0)$ follows from the determinant of the second matrix in Eq. (B5), which must be zero.

In this appendix, we consider the free energy of a microphase in which λ_1 is negative and the other eigenvalues λ_2, λ_3, λ_{10}, and λ_{20} are still positive. When the Landau free energy is minimized, the so-called primary eigenvector $\underline{x}_1$ of λ_1 contributes most and dominates over the much smaller contributions of the other so-called secondary eigenvectors $\underline{x}_2$, $\underline{x}_3$, $\underline{x}_{10}$, and $\underline{x}_{20}$ of λ_2, λ_3, λ_{10}, and λ_{20}, respectively. These secondary contributions are generated by the primary contribution according to Eq. (B12), which is derived later on. From the first and second matrix of Eq. (B5), we easily derive a set of normalized eigenvectors $\widehat{x}_n = (\widehat{\Psi}_n, \widehat{Y}_n^A, \widehat{Y}_n^B)$ with $n = 1, 2, 3, 10,$ or 20. By choosing a fixed set of $\{\widehat{x}_n | n \in \{1,2,3,10,20\}\}$, the Landau free energy can be expressed in terms of parameters $x_1 = \pm|\underline{x}_1|$, $x_2 = \pm|\underline{x}_2|$, $x_3 = \pm|\underline{x}_3|$, $x_{10} = \pm|\underline{x}_{10}|$, and $x_{20} = \pm|\underline{x}_{20}|$ so that it is only minimized with respect to the magnitude of the eigenvectors with an additional plus–minus sign,

$$\frac{F_L}{V} = \min_{\{x_1,x_2,x_3,x_{10},x_{20}\}} \left\{ \lambda_1 x_1^2 + \lambda_2 x_2^2 + \lambda_3 x_3^2 + \lambda_{10} x_{10}^2 + \lambda_{20} x_{20}^2 \right.$$
$$\left. + C_{111}^{(3)} x_1^3 + C_{112}^{(3)} x_1^2 x_2 + \cdots C_{1111}^{(4)} x_1^4 + \cdots \right\}. \qquad (B10)$$

In Eq. (B10), only $C_{111}^{(3)}$, $C_{112}^{(3)}$, etc. and $C_{1111}^{(4)}$, $C_{1112}^{(4)}$, etc. depend on $\{\widehat{x}_n | n \in \{1,2,3,10,20\}\}$. Some examples of these C's are

$$C_{112}^{(3)} = \widetilde{\Gamma}_{\alpha\beta\gamma}^{(3)} \widehat{Y}_1^\alpha \widehat{Y}_1^\beta \widehat{Y}_2^\gamma + \widetilde{\Gamma}_{\alpha\beta}^{(3)} \widehat{Y}_1^\alpha \widehat{Y}_1^\beta \widehat{\Psi}_2 + 2\widetilde{\Gamma}_{\alpha\beta}^{(3)} \widehat{Y}_1^\alpha \widehat{Y}_2^\beta \widehat{\Psi}_1$$
$$+ \widetilde{\Gamma}_\alpha^{(3)} \widehat{Y}_2^\alpha \widehat{\Psi}_1^2 + 2\widetilde{\Gamma}_\alpha^{(3)} \widehat{Y}_1^\alpha \widehat{\Psi}_1 \widehat{\Psi}_2 + \widetilde{\Gamma}^{(3)} \widehat{\Psi}_1^2 \widehat{\Psi}_2 \qquad (B11a)$$

and

$$C_{11,20}^{(3)} = \widetilde{\Gamma}_{\alpha\beta\gamma}^{(3)} \widehat{Y}_1^\alpha \widehat{Y}_1^\beta \widehat{Y}_{20}^\gamma + 2\widetilde{\Gamma}_{\alpha\beta}^{(3)} \widehat{Y}_1^\alpha \widehat{Y}_{20}^\beta \widehat{\Psi}_1 + \widetilde{\Gamma}_\alpha^{(3)} \widehat{Y}_{20}^\alpha \widehat{\Psi}_1^2, \qquad (B11b)$$

in which $\widetilde{\Gamma}$'s are analogous to Γ's according to Eqs. (B6)–(B8). Before minimizing the free energy with respect to the primary parameter x_1, it is first minimized with respect to the secondary parameters x_2, x_3, x_{10}, and x_{20} at a fixed x_1. Each secondary parameter can be approximated by one term, which is quadratic in x_1,

$$x_n = \frac{-C_{11n}^{(3)} x_1^2}{2\lambda_n} + O(x_1^3) \text{ with } n = 2, 3, 10, \text{ or } 20. \qquad (B12)$$

Equation (B12) follows from the following partial derivatives, which are zero at the minimum:

$$\frac{1}{V}\frac{\partial F_L}{\partial x_n} = 2\lambda_n x_n + C_{11n}^{(3)} x_1^2 + \cdots = 0 \text{ with } n = 2, 3, 10, \text{ or } 20. \qquad (B13)$$

Inserting Eq. (B12) into Eq. (B10) yields

$$\frac{F_L}{V} = \min_{x_1} \left\{ \lambda_1 x_1^2 + C_{111}^{(3)} x_1^3 + \left(C_{1111}^{(4)} - \sum_{n \neq 1} \frac{(C_{11n}^{(3)})^2}{4\lambda_n} \right) x_1^4 \right\}$$
$$= \min_{x_1} \{\lambda_1 x_1^2 + C_{111}^{(3)} x_1^3 + \widetilde{C}_{1111}^{(4)} x_1^4\}. \qquad (B14)$$

In this expression, we see that the quadratic term in Eq. (B12) gives a fourth order contribution to the free energy. Hence, other terms with x_1^3 and higher powers in Eq. (B12) can be ignored. When $\lambda_1 < 0$, the value of x_1 at which the minimum is reached can easily be calculated from Eq. (B14), which is

$$x_1 = \frac{-3C_{111}^{(3)} \pm \sqrt{9(C_{111}^{(3)})^2 - 32\lambda_1 \widetilde{C}_{1111}^{(4)}}}{8\widetilde{C}_{1111}^{(4)}}. \qquad (B15)$$

Earlier in the Introduction in Sec. I, we presented the main parameters, such as the bending stiffness λ_α of a block of kind α. The eigenvalues and coefficients in Eq. (B10) depend on these main parameters, but it is not possible to derive expressions in which the eigenvalues and coefficients are explicitly written in terms of

these main parameters especially due to the complexity of the single-chain correlation functions, see Secs. I and IV of the supplementary material, and vertices, see Sec. II of the supplementary material.

To calculate the phase diagram first, the second, third, and fourth order single-chain correlation functions are calculated. In the second order single-chain correlation functions according to Eqs. (I.30a)–(I.30c) of the supplementary material, integrals over the contour lengths l_1 and l_2 are carried out using a Gauss–Jacobi integration.[82] The same method is applied to the third and fourth order single-chain correlation functions. The next step is to calculate the second, third, and fourth order vertices in Eqs. (II.14)–(II.16) of the supplementary material using the resulting single-chain correlation functions in the previous step. Next, second order vertices are inserted in the matrix equation, Eq. (B5), which result in the eigenvalues, eigenvectors, and q_* as explained earlier in this appendix. By means of the eigenvalues, eigenvectors, q_*, and third order and fourth order vertices, the remaining third and fourth order coefficients, see, for example, Eqs. (B11a) and (B11b), are calculated. These remaining third and fourth order coefficients yield the free energy according to Eq. (B14). Each phase structure results in a different free energy with a different minimum. In each point in the phase diagram, the minima of the structures are compared. The phase with the lowest minimum determines the state of the melt.

APPENDIX C: SPACE DEPENDENT ORIENTATION

In this appendix, it is explained how the orientation tensor can be composed if the alignment is space dependent. As mentioned earlier in Appendix B in the first harmonics approximation in Eq. (B2), the orientation tensor has a fixed director vector $\underline{\eta}_\alpha = \underline{\eta}$ so that it can only be used for the nematic phase and layered structures. However, in the bcc and hexagonal phase, we need a director with a variable direction for which an alternative tensor is constructed.

First, we consider the macroscopic alignment $\underline{\underline{Q}}^\alpha(\underline{x})$ in real space,

$$\underline{\underline{Q}}^\alpha(\underline{x}) = \langle \underline{\underline{\widehat{Q}}}^\alpha(\underline{x}) \rangle = Q^\alpha(\underline{x})\left(\underline{\eta}^\alpha(\underline{x})\underline{\eta}^\alpha(\underline{x}) - \frac{1}{3}\underline{\underline{I}}\right), \quad \text{(C1)}$$

in which $\underline{\underline{\widehat{Q}}}^\alpha(\underline{x})$ is the microscopic alignment according to Eq. (8) and $\langle \underline{\underline{\widehat{Q}}}^\alpha(\underline{x}) \rangle$ is the alignment on the coarse-grained level. The space dependent director of blocks of kind α with a fixed unit magnitude is denoted by $\underline{\eta}^\alpha(\underline{x})$. The factor $Q^\alpha(\underline{x})$ determines how strong the α-blocks orient on average with respect to the director. When $Q^\alpha(\underline{x}) > 0$, they tend to align along $\underline{\eta}^\alpha(\underline{x})$. Otherwise, when $Q^\alpha(\underline{x}) < 0$, the alignment is perpendicular to $\underline{\eta}^\alpha(\underline{x})$. Exactly at $Q^\alpha(\underline{x}) = 0$, there is no preferred direction of orientation.

In the nematic phase and layered structures, only one fixed director $\underline{\eta}^\alpha(\underline{x}) = \underline{\eta}^\alpha$ is necessary to describe alignment by Eq. (C1). In that case, the Fourier transform of Eq. (C1) leads to Eq. (B2). In the hexagonal and bcc phase, the symmetrical properties would be lost when using one fixed director. In these structures, the chains tend to align in multiple directions for which a tensor other than Eq. (B2) has to be found. To solve this problem, we assign to $\underline{\eta}^\alpha(\underline{x})$ a fixed unit vector only on a local level.

For example, in Fig. 6, for the hexagonal state, several areas have been drawn with fixed directors restricted to three possible
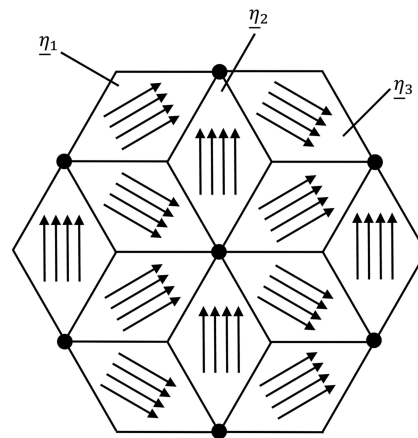

FIG. 6. Director field $\underline{\eta}(\underline{x})$ in the plane perpendicular to the cylinders in the hexagonal phase.

directions $\underline{\eta}_1$, $\underline{\eta}_2$, and $\underline{\eta}_3$. At the dots, we are in the center of a cylinder with a slightly higher concentration of blocks of kind α. The lines enclose areas with a fixed director, which are indicated by V_{1n}, V_{2n}, and V_{3n} containing director $\underline{\eta}_1$, $\underline{\eta}_2$, and $\underline{\eta}_3$, respectively, and $n = 1, 2, \ldots$, so

$$\underline{\eta}^\alpha(\underline{x}) = \begin{cases} \underline{\eta}_1 & \text{if } \underline{x} \in V_{1n}, \\ \underline{\eta}_2 & \text{if } \underline{x} \in V_{2n}, \\ \underline{\eta}_3 & \text{if } \underline{x} \in V_{3n}. \end{cases} \quad \text{(C2)}$$

In Eq. (C2), the directions of $\underline{\eta}_1$, $\underline{\eta}_2$, and $\underline{\eta}_3$ are identical to the directions of the wave vectors in set $H_{hex} = \{\pm\underline{q}_1, \pm\underline{q}_2, \pm\underline{q}_3\}$, which are applied in Eqs. (B1) and (B2). Applying Eq. (C2) in Eq. (C1) and carrying out a Fourier transformation lead to

$$\underline{\underline{Q}}^\alpha_{hex}(\underline{q}) = \frac{1}{3}\sum_{m=1}^{3}\underline{\underline{Q}}^\alpha_{smecA}(\underline{q}, \underline{\eta}_m). \quad \text{(C3)}$$

In this form, we are averaging three smectic-A phases with directors $\underline{\eta}_1$, $\underline{\eta}_2$, and $\underline{\eta}_3$, which yield an alignment description $\underline{\underline{Q}}^\alpha_{hex}$ of the hexagonal phase. Analogously, we derive the description $\underline{\underline{Q}}^\alpha_{bcc}$ of the bcc structure,

$$\underline{\underline{Q}}^\alpha_{bcc}(\underline{q}) = \frac{1}{6}\sum_{m=1}^{6}\underline{\underline{Q}}^\alpha_{smecA}(\underline{q}, \underline{\eta}_m), \quad \text{(C4)}$$

in which the six directors $\underline{\eta}_m$ must be parallel to the wave vectors in set H_{bcc}. According to Eq. (B2), the alignments $\underline{\underline{Q}}^\alpha_{smecA}(\underline{q}, \underline{\eta}_m)$ contain phase factors $\exp(i\varphi_q)$, which are, therefore, also in $\underline{\underline{Q}}^\alpha_{hex}(\underline{q})$ and $\underline{\underline{Q}}^\alpha_{bcc}(\underline{q})$. These phase factors must conform the symmetry of the structure.

REFERENCES

[1] J. J. M. Slot, H. J. Angerman, and G. ten Brinke, J. Chem. Phys. **109**(19), 8677 (1998).

[2] H. J. Angerman, G. ten Brinke, and J. J. M. Slot, Eur. Phys. J. B **12**, 397 (1999).

[3] H. J. Angerman, G. ten Brinke, and I. Erukhimovich, Macromolecules **29**, 3255 (1996).

[4] H. J. Angerman, Ph.D. thesis, University of Groningen, 1998.

[5] L. Leibler, Macromolecules **13**, 1602 (1980).

[6] M. Reenders and G. ten Brinke, Macromolecules **35**, 3266 (2002).

[7] P. Friedel, A. John, D. Pospiech, D. Jehnichen, and R. R. Netz, Macromol. Theory Simul. **11**(7), 785 (2002).

[8] C. Singh, M. Goulian, A. J. Liu, and G. H. Fredrickson, Macromolecules **27**, 2974 (1994).

[9] R. Holyst and M. Schick, J. Chem. Phys. **96**(1), 7728 (1992).

[10] S.-H. Wang, T. Kawakatsu, P. Chen, and C.-Y. D. Lu, J. Chem. Phys. **138**, 194901 (2013).

[11] A. Werner and G. H. Fredrickson, J. Polym. Sci., Part B: Polym. Phys. **35**(5), 849 (1997).

[12] A. Aksimentiev and R. Hołyst, J. Chem. Phys. **111**(5), 2329 (1999).

[13] M. Hernández-Jiménez and H. Westfahl, Jr. Eur. Phys. J. E **23**, 31 (2007).

[14] A. John, P. Friedel, D. Pospiech, D. Jehnichen, and C. Kunert, Macromol. Theory Simul. **13**(8), 702 (2004).

[15] C. Burger, W. Ruland, and A. N. Semenov, Macromolecules **23**, 3339 (1990).

[16] G. H. Fredrickson and E. Helfand, J. Chem. Phys. **87**(1), 697 (1987).

[17] M. A. Aliev and N. Y. Kuzminyh, J. Chem. Phys. **143**, 084901 (2015).

[18] M. A. Aliev, N. Y. Kuzminyh, and E. A. Ugolkova, Physica A **392**(24), 6214 (2013).

[19] M. W. Matsen, J. Chem. Phys. **104**(19), 7758 (1996).

[20] M. W. Matsen, J. Chem. Phys. **108**(2), 785 (1998).

[21] M. W. Matsen and R. B. Thompson, J. Chem. Phys. **111**(15), 7139 (1999).

[22] M. W. Matsen, J. Phys.: Condens. Matter **14**, R21 (2002).

[23] M. W. Matsen and M. Schick, Phys. Rev. Lett. **72**, 2660 (1994).

[24] S. W. Sides and G. H. Fredrickson, J. Chem. Phys. **121**(10), 4974 (2004).

[25] J.-Z. Chen, C.-X. Zhang, Z.-Y. Sun, L.-J. An, and Z. Tong, J. Chem. Phys. **127**, 024105 (2007).

[26] Y. Xia, J. Chen, Z. Sun, T. Shi, L. An, and Y. Jia, Polymer **51**, 3315 (2010).

[27] J. Tang, Y. Jiang, X. Zhang, D. Yan, J. Z. Y. Chen, and Y. Chen, Macromolecules **48**, 9060 (2015).

[28] Y. Xia, J. Chen, Z. Sun, T. Shi, L. An, and Y. Jia, J. Chem. Phys. **131**, 144905 (2009).

[29] W. Song, P. Tang, F. Qiu, Y. Yang, and A.-C. Shi, Soft Matter **7**, 929 (2011).

[30] W. Song, P. Tang, F. Qiu, Y. Yang, and A.-C. Shi, J. Phys. Chem. B **115**, 8390 (2011).

[31] Y. A. Kriksin, S.-H. Tung, P. G. Khalatur, and A. R. Khokhlov, Polym. Sci., Ser. C **55**(1), 74 (2013).

[32] E. W. Cochran, C. J. Garcia-Cervera, and G. H. Fredrickson, Macromolecules **39**(7), 2449 (2006).

[33] W. Song, P. Tang, H. Zhang, Y. Yang, and A.-C. Shi, Macromolecules **42**, 6300 (2009).

[34] J. Yu, F. Liu, P. Tang, F. Qiu, H. Zhang, and Y. Yang, Polymers **8**, 184 (2016).

[35] Y. Jiang and J. Z. Y. Chen, Acta Phys. Sin. **65**(17), 178201 (2016).

[36] M. A. Osipov and M. V. Gorkunov, Phys. Rev. E **100**, 042701 (2019).

[37] M. A. Osipov, M. V. Gorkunov, A. V. Berezkin, A. A. Antonov, and Y. V. Kudryavtsev, J. Chem. Phys. **152**, 184906 (2020).

[38] J. Song, T. Shi, Y. Li, J. Chen, and L. An, Chem. Phys. **129**, 054906 (2008).

[39] A. V. Berezkin, Y. V. Kudryavtsev, and M. A. Osipov, Polym. Sci., Ser. A **62**(4), 430 (2020).

[40] T. Ohta, N. Yamazaki, M. Motoyama, K. Yamada, and M. Nonomura, J. Phys.: Condens. Matter **17**, S2833 (2005).

[41] B. D. Olsen and R. A. Segalman, Macromolecules **38**, 10127 (2005).

[42] B. D. Olsen and R. A. Segalman, Macromolecules **39**, 7078 (2006).

[43] B. D. Olsen, M. Shah, V. Ganesan, and R. A. Segalman, Macromolecules **41**, 6809 (2008).

[44] N. Sary, C. Brochon, G. Hadziioannou, and R. Mezzenga, Eur. Phys. J. E **24**, 379 (2007).

[45] B. Olsen and R. Segalman, Mater. Sci. Eng., R **62**, 37 (2008).

[46] I. W. Hamley, *The Physics of Block Copolymers* (Oxford University Press, Oxford, 1998).

[47] P. J. Flory, *Principles of Polymer Chemistry* (Cornell University Press, Ithaca, NY, 1953).

[48] A. N. Semenov and A. R. Khokhlov, Sov. Phys.-Usp. **31**, 988 (1988).

[49] A. R. Kokhlov and A. N. Semenov, Macromolecules **19**, 373 (1986).

[50] W. Maier and A. Saupe, Z. Naturforsch., A: Phys. Sci. **13**, 564 (1958).

[51] J. B. Lagowski, J. Noolandi, and B. Nickel, J. Chem. Phys. **95**(2), 1266 (1991).

[52] M. Bixon and R. Zwanzig, J. Chem. Phys. **68**(4), 1896 (1978).

[53] M. G. Bawendi and K. F. Freed, J. Chem. Phys. **83**(5), 2491 (1985).

[54] R. A. Harris and J. E. Hearst, J. Chem. Phys. **44**(7), 2595 (1966).

[55] N. Saitô, K. Takahashi, and Y. Yunoki, J. Phys. Soc. Jpn. **22**(1), 219 (1967).

[56] K. F. Freed, Adv. Chem. Phys. **22**, 1 (1972).

[57] A. M. Gupta and S. F. Edwards, J. Chem. Phys. **98**(2), 1588 (1993).

[58] P. M. Jager, "Effects of stiffness and polydispersity on the phase behaviour of block copolymers," Ph.D. thesis, University of Twente, The Netherlands, 2006.

[59] I. M. Lifshitz, A. Y. Grosberg, and A. R. Khokhlov, Rev. Mod. Phys. **50**, 683 (1978).

[60] N. G. van Kampen, *Stochastic Processes in Physics and Chemistry* (North-Holland, Amsterdam, 1981).

[61] P. M. Chaikin and T. C. Lubensky, *Principles of Condensed Matter Physics* (Cambridge University Press, Cambridge, 1995).

[62] J. C. Toledano and P. Toledano, *The Landau Theory of Phase Transitions* (World Scientific, Singapore, 1987), Vol. 3.

[63] S. V. Panyukov and S. I. Kuchanov, J. Phys. II (France) **2**, 1973 (1992).

[64] E. I. Shakhnovich and A. M. Gutin, J. Phys. (France) **50**, 1843 (1989).

[65] G. H. Fredrickson, S. T. Milner, and L. Leibler, Macromolecules **25**, 6341 (1992).

[66] G. H. Fredrickson and L. Leibler, Macromolecules **23**, 531 (1990).

[67] G. H. Fredrickson and S. W. Sides, Macromolecules **36**, 5415 (2003).

[68] M. Foroutan and M. A. Jafarizadeh, Physica A **307**, 221 (2002).

[69] M. Foroutan and M. A. Jafarizadeh, Physica A **329**, 337 (2002).

[70] S. Panyukov and I. Potemkin, Physica A **249**, 321 (1998).

[71] I. I. Potemkin and S. V. Panyukov, Phys. Rev. E **57**(6), 6902 (1998).

[72] A. M. Gutin, C. D. Sfatos, and E. I. Shakhnovich, J. Phys. A: Math. Gen. **27**, 7957 (1994).

[73] A. Nesarikar, M. Olvera de la Cruz, and B. Crist, J. Chem. Phys. **98**(9), 7385 (1993).

[74] A. V. Dobrynin and L. Leibler, Macromolecules **30**, 4756 (1997).

[75] V. Abetz, R. Stadler, and L. Leibler, Polym. Bull. **37**, 135 (1996).

[76] I. Erukhimovich, V. Abetz, and R. Stadler, Macromolecules **30**, 7435 (1997).

[77] S.-M. Mai, W. Mingvanish, S. C. Turner *et al.*, Macromolecules **33**, 5124 (2000).

[78] X. Ren and J. Wei, Physica D **178**, 103 (2003).

[79] E. W. Cochran, D. C. Morse, and F. S. Bates, Macromolecules **36**, 782 (2003).

[80] K. M. Jaffer, R. A. Wickham, and A.-C. Shi, Macromolecules **37**, 7042 (2004).

[81] P. P. F. Wessels and B. M. Mulder, Phys. Rev. E **70**, 031503 (2004).

[82] W. H. Press, S. A. Teukolsky, and W. T. Vetterling, *Numerical Recipes in C*, 2nd ed. (Cambridge University Press, Cambridge, 1996).

10 April 2024 11:34:15